EFFECT OF LOW CYCLE FATIGUE DAMAGE ON TENSILE BEHAVIOR OF SENSITIZED STAINLESS STEEL

Thesis submitted in partial fulfilment of the requirements for the award of the degree of

Master of Technology

in

Mechanical Engineering

[Specialization**:** Steel Technology]

Submitted by

MD. AFZAL HUSSAIN

Roll No.-**212MM2455**

Department of Metallurgical and Materials Engineering

National Institute of Technology

Rourkela-769008, (India)

May 2014

EFFECT OF LOW CYCLE FATIGUE DAMAGE ON TENSILE BEHAVIOR OF SENSITIZED STAINLESS STEEL

Thesis submitted in partial fulfilment of the requirements for the award of the degree of

Master of Technology

in

Mechanical Engineering

[Specialization**:** Steel Technology]

Submitted by

MD. AFZAL HUSSAIN

Roll No.-**212MM2455**

Under the Supervision of

Prof. Krishna Dutta

Department of Metallurgical and Materials Engineering

National Institute of Technology

Rourkela-769008, (India)

May 2014

Dedicated to

my parents Mr. Ismail Ansari and Mrs. Marjun Nisa, and my sister Mrs. Yasira Khatoon

Department of Metallurgical and Materials Engineering

National Institute of Technology, Rourkela, Odisha-769008, India

CERTIFICATE

This is to certify that the thesis entitled "**Effect of Low Cycle Fatigue Damage on Tensile Behavior of Sensitized Stainless Steel**" submitted by **MD. AFZAL HUSSAIN,** Roll No.-**212MM2455** in partial fulfilment of the requirements for the award of the degree of Master of Technology in **Mechanical Engineering** with Specialization of **Steel Technology** at National Institute of Technology, Rourkela is an authentic work carried out by him under my supervision and guidance.

To the best of my knowledge, the matter embodied in the thesis has not been submitted to any other university/institute for the award of any degree or diploma.

Date:

Place: Rourkela

Supervisor

Prof. Krishna Dutta

Department of Metallurgical and Materials Engineering

National Institute of Technology,

Rourkela-769008

Acknowledgement

I thank **Dr. Bankim Chandra Ray**(HOD, Department of Metallurgical and Materials Engineering, NIT Rourkela) for having provided me the opportunity to do this project work.

I would like to take this opportunity to express my sincerest and utmost gratitude to my supervisor **Prof. Krishna Dutta**,Department of Metallurgical and Materials Engineering, NIT Rourkela, for his exemplary guidance, valuable suggestions, and his incredible patience and for having taught and supported me at every turn in my endeavour throughout the research project work. The help and guidance given by him time to time shall carry us a long journey ahead. It would have not been possible for me to carry out this thesis deprived of his assistance and constant encouragement. He has spent so much time helping me clarify my thoughts when I encountered confusion. I never thought this complicated thesis would be finished until the very last minute. His valuable and insightful review provided constructive feedback to my drafts. I really appreciate his dedication to this thesis.

I would deliver my enormous thankfulness to **Dr. B.B. Verma**(Professor, Department of Metallurgical and Materials Engineering, NIT Rourkela) and other faculty members of this department for their tenacious support and instruction to finish the research work.

Last but not the least, I am highlythankful to laboratory members, Department of Metallurgical and Materials Engineering, NIT Rourkela, specially Mr. S. Hembram, Mr. A. Pal, Mr. R. Pattanaik, Mr. K. Tanty and my friends Om Prakash Tenduwe and HemantNautiyal for their assistance during tensile and LCF tests and the entire technical staff of this department for their direct and indirect help during the execution of experiment.

A special thanks to Mr. S. Chakraborty for his assistance in undertaking the FESEM analysis.

Finally, I am grateful to all my classmates and friends who made my stay in Rourkela, a memorable and pleasing experience.

Place: Rourkela **Md. Afzal Hussain**

Abstract

The aim of this report is to effect of sensitization treatment of the low cycle fatigue and post-fatigue tensile properties of a non-conventional austenitic stainless steel. The metallurgical investigation of solution annealed as well as sensitizedstainless steels were carried out in order to determine the microstructural characteristics, hardness, grain size distribution, tensile and low cycle fatigue properties and finally to determine the dislocation densities of the deformed specimens. The microstructure of the selected steel in solution annealed condition reveals that the steel owns nearly equiaxed austenite grains with annealing twins throughout the matrix. The grain size measurement was carried out by the aid of line intercept method for all materials and average grain size of as-received steel was found 23.49 ± 4.40 μm. Tensile and low cycle fatigue tests of the samples were carried out by using universal testing machine of ±100 kN capacity. The results indicate that the steel cyclically softens in both solution annealed as well as sensitized conditions. This nature of softening is also seen in the post-fatigue tensile tested samples. The fractographic analyses indicate that the fracture surfaces of the sensitized specimens are predominantly of typical rock candy type fracture whereas dimple fracture was observed in the solution annealed sample. Typical dislocation density in the deformed specimen assessed by X-ray diffraction profile analyses, is 6.2804×10^{15} m^{-2} in case of solution annealed sample while in sensitized steel specimens this range is 9.0575×10^{14} m^{-2}. Thus, an increase of nearly an order of magnitude in the dislocation density was found.

Key words: Sensitization, non-conventional stainless steel, low cycle fatigue, dislocation density.

CONTENTS

LIST OF FIGURES

LIST OF TABLES

Nomenclatures

d	Average grain size, μm
N_L	Number of grains intercepted by a unit true test line length
L_T	True length of test line
K	Kelvin
P	Applied Load
d_{avg}	Average sum of indentation diagonals
d_1, d_2	Length of indentation diagonals
σ_{max}	Maximum Stress
σ_{min}	Minimum stress
σ_r	Stress range
σ_a	Alternating stress
σ_m	Mean stress
R	Stress ratio
A	Amplitude ratio
θ	Diffraction angle
λ	Wavelength of XRD profiles
b	Berger's vector
ρ	Dislocation density
$\Delta(2\theta)$	Integral breadth (FWHM)
M	Constant, effective outer cut-off radius of dislocations and dislocation density
C	Average contrast factor of the dislocations
$\overline{C}$	Average contrast factor of the dislocation of all intensity peaks
C_{h00}	Average contrast factor corresponding to h00 reflection
t	time
$\%\varepsilon_t$	%total elongation
$\%\varepsilon_u$	%uniform elongation
N	Number of cycles
$d\varepsilon/d_t$	Strain rate

Abbreviations

AISI	American Iron and Steel Institute
SS	Stainless steel
XRD	X-ray diffraction
fcc	Face centered cubic
UTS	Ultimate tensile strength
FESEM	Field emission scanning electronmicroscope
VLCF	Very high cycle fatigue
VHCF	Very low cycle fatigue
YS	Yield strength
Hv	Vickers hardness
FWHM	Full width half maximum
HCF	High cycle fatigue
LCF	Low cycle fatigue
UE	Uniform elongation
TE	Total elongation
IGSCC	Intergranular stress corrosion cracking
IGC	Intergranular corrosion
GBE	Grain boundary engineering
FCGR	Fatigue crack growth rate
XRD	X-ray diffraction
OES	Optical emission spectroscopy

Chapter 1

Introduction

Outline

Introduction

Objectives of the work

Organisation of thesis

1.1 Introduction

Austenitic stainless steels establish the biggest stainless (i.e. rusting) family in terms of number of alloys and their usage. The austenitic alloys are nonmagnetic with excellent ductility, toughness even at cryogenic temperatures [1]. Nickel is the key element used to stabilize austenite while role of carbon and nitrogen are readily soluble in the face centered cubic (fcc) structure. These steels have a wide range of applications, from domestic appliances, household utensils, electrical and electronic appliances to the cutlery industries, food and beverage industries, chemical, petrochemical, nuclear, transportation and architecture industries owing to its outstanding combination of oxidation and corrosion resistance, mechanical properties under the monotonic and cyclic loading states [1, 2]. Despite the various grades of stainless steel, austenitic stainless steels have face centered cubic (fcc) lattice structure which is stable from the ambient temperature to the melting temperature. The non-conventional special grade of austenitic stainless steel is also designated as ISO/TR 15510 X12CrMnNiN17-7-5, used for manufacturing components such as trim, wheel covers, flat conveyer chains, railroad passenger car bodies etc. These steels are being produced to conserved nickel [1]. Apart from various beneficial effects, the main adverse effect of stainless steel is its sensitization. The phenomenon of sensitization is a commonly encountered problem associated with the service of the non-conventional stainless steels [33].These steels are used in superheaters and reheaters. For high-temperature boiler applications, three general grades, 304, 321, and 347, are the most widely used. It can be mentioned here that in almost all the above mentioned applications, failure of components by fatigue is one of the major deformation mechanisms. But as per the knowledge of the current investigators the extent of work performed on fatigue and post fatigue tensile behavior of sensitized stainless steel is almost negligible. Therefore, it is required to study the low cycle fatigue behavior of sensitized stainless steel and its consequences on post tensile properties.

In this investigation the low cycle fatigue experiments under three different strain amplitudes for solution annealed and sensitized (1 hr., 3 hrs., 5 hrs. and 7 hrs.) stainless steel samples upto 100 cycles has been carried out. These have been followed by tensile tests on the fatigued samples. Fractographic analyses have been done to understand the variations in fracture surface morphologies of the failed samples. X-ray diffraction profiles analyses have also been done to assess the dislocation density in all the specimens, using the modified Williamson Hall expression [44] for all deformed samples.

1.2 Objectives of the work

The main objectives and related work strategies to achieve these can be briefly summarized as:

(I) To impose sensitization effect to the selected non-conventional austenitic stainless steel: This part consists of imposing sensitization effect to the steel by holding it at a certain temperature for different periods of time.

(II) To characterize the selected steel in solution annealed and sensitized conditions: This part comprises of (a) microstructural characterization of both the solution annealed and sensitized condition, (b) measurement of grain size and their distribution, (c) determination of micro and macro hardness, (d) determination of tensile properties at room temperature.

(III) To study the low cycle fatigue and post fatigue tensile behavior of the selected steel: In this part, low cycle fatigue tests have been carried out under three different strain amplitudes for each set of specimens. Tensile tests have been also been done after 100 fatigue cycles on these samples. The fracture surfaces have been investigated for all the deformed specimens.

(IV) To estimate the dislocation density of the selected steel: The dislocation densities have been estimated on the solution annealed and sensitized steel in both before and after fatigue tests.

1.3 Organisation of thesis

Thesis comprises of five chapters excluding references which are mentioned in brief as below:

Chapter-1 contracts the general background of austenitic stainless steel and its applications in industries and structural design field. A discussion is made in this section of their significance of the problem with emphasis on fatigue behavior and motivation behind this research. Apart from these, objectives of the present research work are included in this section.

Chapter-2 delivers a critical review of the existing literature associated to the effect of sensitization on cyclic loading, nature of cyclic hardening/softening, fatigue behavior and tensile properties affected by low cycle fatigue with an objective to analyse the controversies

and unsolved issues. The evidence in the published literature raises unanswered queries but the available journals provide the routes for further research.

Chapter-3 deals with a comprehensive explanation of the experiments, which have been carried out during the investigation.

Chapter-4 comprises the results and discussion related to the present research work.

Chapter-5 includes results and discussion of the present work strained from the investigations. Some of proposed future work associated to this domain has been accumulate at the very end of this chapter.

All the references cited throughout the thesis are enlisted after chapter-5.

Chapter 2

Literature Survey

Outline

Stainless steel-An over view

Sensitization of stainless steel

Fatigue- General aspects

Cyclic stresses

Fatigue cycling- Different extents

- **High cycle fatigue**
- **Very high cycle fatigue**
- **Low cycle fatigue**
- **Very low cycle fatigue**

Literatures available related to sensitization of stainless steel

Some pertinent literatures on low cycle fatigue of Stainless steel

Some pertinent literatures associated with estimation of dislocation density of stainless steel

2.1 Stainless Steel-An Over View

The discovery of stainless steel came out when French, German, English and later U.S. metallurgist started getting the results of their studies on low carbon chromium containing ferrous alloy.

In between 1904-1909, French metallurgist Leon B. Guillet and Albert M. Portevin published a series of studies on the structure and properties of 13% Cr martensitic and 17% Cr ferritic steels containing from 0.12 to 1.0% C. In 1909, Guillet and the German metallurgist W. Giesen published studies on iron- Chromium-nickel based austenitic alloys.In 1908 in Germany, Philipp Monnartz studied the role of carbon content on the corrosion resistance of iron-chromium steels. His research disclosed that the "stainless" (inoxydable in French or rostfrei in German) quality of these materials was a function of the passivity phenomenon [1].

In the United States wrought grades of stainless steels are generally entitled by American Iron and Steel Institute (AISI) numbering system, the Unified numbering system (UNS), or the proprietary name of the alloy. These numbering systems are older and widely used. Most of the stainless steel grades have three digit designation, the 200 and 300 series are generally austenitic stainless steels, whereas the 400 series are either ferritic or martensitic [1].

The stainless steel are iron base alloys greatly resistant to rusting in a variety of environments, especially the ambient atmosphere. Main alloying element of stainless steel is is chromium and at least 11 wt. % Cr concentrations are required to prevent the formation of rust in unpolluted environments. It brings their "stainless" characteristics by forming of an invisible and adherent chromium rich oxide surface film. Besides this, corrosion resistance may be enhanced by the addition of nickel and molybdenum [1]. Other elements like silicon, copper, aluminium, titanium, niobium, nitrogen, sulphur, and selenium is added to enhance particular quality.

Stainless steel are classified into five categories on the base of the predominant phase constituent of the microstructure-martensitic, ferritic and austenitic, duplex and precipitation-hardenable stainless steel.

- ✧ Martensitic stainless steels-These consist 12-17% chromium and 0.10 to 1.20% carbon. These steels heat treatable type and shows austenitic nature at temperatures of 950-1000 ^{o}C, while on cooling transform to martensite.

- ✧ Ferritic stainless steels- These possess 11.5 to 27% chromium and carbon content is kept 0.08 to 0.2% to improve toughness as well as reduce sensitization. It exhibits ferritic in structure up to melting point.
- ✧ Austenitic stainless steels-These consist 16-25% chromium, 8-20% nickel and 0.03-0.10% carbon and exhibits austenitic at room temperature.
- ✧ Duplex stainless steels- These are the combination of ferritic and austenitic and phase proportion is controlled by heat treatment. These possess 23-30% chromium, 2.5-7% nickel and some amount of titanium or molybdenum.
- ✧ Precipitation-hardenable stainless steels- These are chromium-nickel based alloy and can be hardened by age treatment which offer attractive combinations of properties. These are quite expensive and used in high temperature applications.

The physical and mechanical properties of stainless steels are quite different from non-ferrous alloys. Stainless steels have properties like corrosion and oxidation resistance, creep strength, hardness, ductility, formability, appearance etc. Thus, from domestic items (wash basin, utensils, cutlery items etc.) to heat exchanger, pressure vessels, springs, surgical tools, bearings, combustion chamber, cryogenic vessels, piping, storage tanks in chemical industries, to structural materials used in nuclear reactor, materials for chemical processing plants, food processing equipment etc. are wide range of applications [1,2].

Table 2.1: Classification of stainless steel based on their elemental compositions.

TYPES	MAJOR ALLOYING ELEMENTS (%)									Others (%)
	C	Mn	Si	P	S	Cr	Ni	Mo	N	
Ferritic	0.08-0.2	1-2.5	1	0.04-0.06	0.03-0.06	11.5-27	0.5	0.6-2.5	Min 0.025	Al, Se, Cu, Ti
Martensitic	0.15-1.2	1-2.5	0.5-1	0.04-0.06	0.03-0.35	11.5-18	0.75-2.5	0.4-1	Min 0.08	
Austenitic	0.03-0.25	2-19	4.5	0.03-0.17	0.03-0.35	11.5-23	2.5-38	0.5-3	0.08-0.4	Nb, Zr, V are also present in trace amounts
Duplex	0.02-0.04	1-2	0.75-1	0.03-0.04	0.01-0.03	21-26	2.5-6.5	1-4	0.08-0.35	
Precipitation Hardenable	0.05-0.15	0.2-1.25	0.1-1	0.01-0.04	0.008-0.04	11-18	3.5-27	0.5-3.25	0.01-0.13	

2.2 Sensitization of Stainless Steel

The concept of chromium depletion of sensitization of austenitic stainless steels was first assumed by Strauss et al. [4] and Bain et al.[9] and they have been suggested numerous other models. However, these models have appreciated little experimental support and almost all have been rejected as written by P. J. Gellings and M. A. Dejongh [3]. The utility of a quantitative theory of sensitization would comprise its capability to forecast the degradation i.e. whether a material would deteriorate in particular alloy like intergranular corrosion and stress corrosion cracking. Eventually, to defend quantitatively the corrosion and stress corrosion cracking actions of stainless steels, chromium depletion model as proposed by Strauss [4] and Bain [9] is essential to raise the improvement in the qualitative. Now a days various models with quantitative protection ability have been projected. The kinetic features of carbide growth and the study related to the formation of chromium depleted zones was focused by Stawstrom and Hillert [5], they analysed time-temperature relation to execute sensitize and to desensitize of 304 stainless steel by the function of carbon and grain size. Tedmon et al. [6] and Fullman [7] have made their concentration on the thermo dynamics features of carbide precipitation and the formation of chromium depleted zones. Their calculations were beyond the function of time –temperature need to sensitize and desensitize of the alloys. The effects of alloying elements and their subsequent variations such as chromium, carbon, nickel, molybdenum, manganese, nitrogen, silicon etc. on the sensitization behavior that can be broadly categorised [8].

It is very fact that when austenitic stainless steels are widely heat treated or cooled slowly in the temperature range from 773 to1173 K, chromium and carbon combine to each other in order to form chromium rich carbides (typically $Cr_{23}C_6$ or $M_{23}C_6$) in the locality of the grain boundaries with the consequent chromium depletion along the grain boundaries. As these carbides form at the grain boundaries, depletion of chromium arises at the adjacent zones. This process is known as sensitisation. It leads to decrease in the corrosion resistance of stainless steel, particularly resistance to intergranular corrosion. This seeks out depleted regions anodic in the presence of an electrolyte [9-11]. Sensitization causes Intergranular corrosion intergranular stress corrosion cracking and embrittlement. If the local chromium possess below 12 wt. %, then the chromium depleted zones become highly susceptible to local corrosion and intergranular stress corrosion cracking (IGSCC), in this sensitization process. When the sensitized material is bring in corrosive media, intergranular corrosion takes place. It often seen that fabricated components are interacted to the sensitization range

during some heat treatments like solution annealing, dimensional stabilization or stress-relieving[12-13]. If the rate of critical cooling is slow during these heat treatments than the material may be sensitized and intergranular corrosion and inter granular stress corrosion cracking come into the picture. But such type of material failures is taken into the account without sensitization during fabrication, pre-commissioning steps and service age. Improper heat treatment of components also brings sensitization during the service life [14–17].

The amount of chromium depletion in a given material can differ from boundary to boundary and even from point to point along the same boundary as confirmed by the outstanding work of Briant and Hall [18]. To estimate the validity of several models of sensitization, the variations in chromium concentration both normal to and along the grain boundaries, a repetitive measurement must be taken for a number of grain boundaries. Additionally, in order to observe the kinetics of sensitization and desensitization such analyses must be made on a number of samples followed by heat treatment at different desired temperatures and time [8].

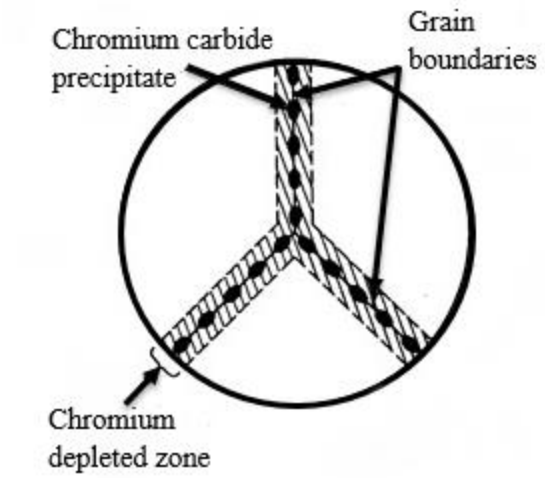

Fig. 2.1: Precipitation of chromium carbide at grain boundary and chromium depleted zone.

Time-temperature-sensitization curves are shown in Fig.2.1. that provide the control for avoiding sensitization and demonstrate the effect of carbon content on this phenomenon.The curve shows that the steel with 0.062% C would have to cool below 595°C within 5 minute to avoid sensitization,but austenitic grades of stainless steel with very low carbon content could take about 20 hours to cool below 480 °C without becoming sensitized [19]. Sensitization can also be avoided by using stabilized steels which contain niobium or titanium, or tantalum.

These elements have an affinity for carbon and thus carbides form easily. Thus Chromium is not depleted and thus it allows chromium to remain in solution even for extremely long exposures to temperatures in the sensitizing range.

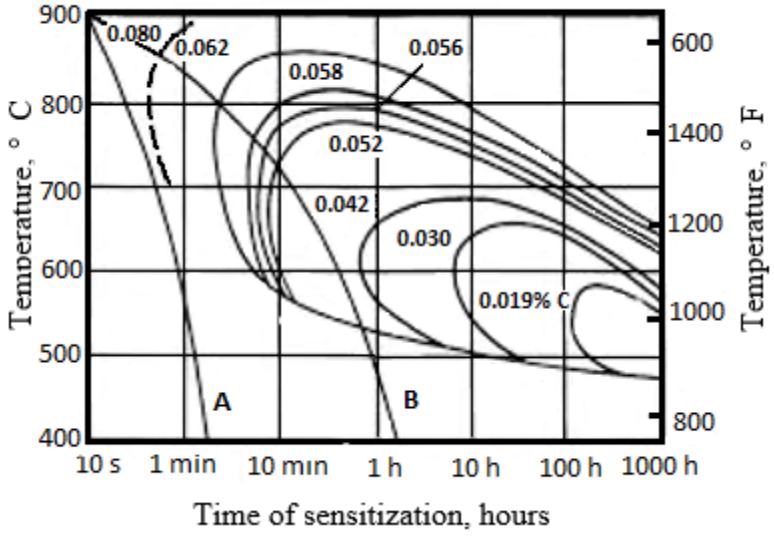

Fig. 2.2: Time –temperature sensitization curves for austenitic stainless steel.

In order to prevent the sensitization effect, various methods have been suggested and few of these are mentioned below:

- To dissolve the carbides formed during sensitization, heat treatment should be done between the temperature ranges of 1223-1373 K followed by rapid cooling.
- The amount of carbon content is reduced to avoid the formation of carbides.
- To increase the molybdenum content in stainless steel.
- The carbide formers like Niobium, titanium or tantalum, its content should be raised.

2.3 Fatigue-General Aspects

In the 1800s, the discovery of fatigue concept came out when some investigators in Europe observed that components of railroad and bridge were failing due to the initiation of cracks when subjected to repeated loading. Undoubtedly, earlier failures caused by cyclic loads was limited due to use of such components as clay pipes, concrete structures and wood structures, investigation of failures were made based on these components. But the requirement of

metallic machines components in late 1800s essential to design the techniques such that it would prevent the failures owing to repeated loads of all kinds of material. From that time to till date the research is still going on fatigue failure even today [20]. During the fatigue process, it meets four different phases as mentioned below:

- Nucleation and growth
- Crack propagation
- Elastic-plastic fracture mechanics
- Final unpredictability

Interest in the avoidance of fatigue failure in structural component initiated with the advent of industrial revolution where mechanical devices were subjected to repetitive load by the nature of their operational condition[21].The structural behavior of any material depends not only upon the character of loads but also upon the nature of the material. Here, according to the situations load may be static or dynamic. In the case of static, loads are applied gradually, act for long spans of time and for dynamic, are impact loads which act suddenly and repeated loads recurring for large number of cycles.

It has been recognized since 1830, when a structure or metal component subjected to dynamic loads is possible to fail at a stress levels much lower than its monotonic fracture strength value while the same amount of loads are applied statically, especially when the loads are repeated or fluctuated for a large number cycles. Fatigue has become increasingly more applicable in developed technology in the areas, such as automobile parts, airplane parts, propellers, shafts, generators, compressors, pumps, turbines and the like. In this day and age, it is often specified that almost 90% of all metallic failures, polymers and ceramics (except for glasses) are also susceptible to this type of failures during their service life, occur due to fatigue [22].The deterioration of a material results progressive cracking that finally produces fracture under a repeated cycles of stress as well as strain and habitually fails at stress levels lower than their monotonic fracture strength point for static load, is called fatigue [23-24]. Followings are three basic factors essential to cause fatigue failure:

- ★ Maximum tensile stress of sufficiently high values.
- ★ Large enough variation and fluctuation in the applied stress.
- ★ Large number of cycles of the stress applied.

Besides these factors, some other variables also take part in order to alter the conditions for fatigue, such as metallurgical structure, residual stresses, combined stresses, stress concentration, corrosion, temperature and overloads. Although, fatigue failures may appear to be abrupt, the route of fatigue fracture is progressive which begins with the initiation of cracks and the cracks propagate during cyclic loading till the rupture of a component or specimen during their service life [22].

2.4 Cyclic Stresses

The applied stress may be axial, flexural, or torsional in nature. Fluctuating stress-time modes are possible in three different habits. Major types of fluctuating stresses which can cause fatigue are cited below:

a) Reversed stress cycle;

b) Repeated stress cycle;

c) Irregular or random stress cycle.

Fig. 2.3 (a) shows schematically which is referred as completely reversed cycle of stress by regular and sinusoidal time dependence. The value of maximum and minimum stresses are of equal magnitude wherein the amplitude is symmetrical about a mean zero stress level (i.e. $\sigma_m = 0$). Positive sign signifies tensile stress as well as negative sign signifies compressive stress. Fig. 2.3 (b) illustrates a repeated stress cycle in which the maximum stress (σ_{max}) and minimum stress (σ_{min}) are not identical. In this figure, both maximum and minimum stress are in tension. This is known as asymmetric loading (i.e. $\sigma_m \neq 0$).Fig. 2.3 (c) represents a complicated stress cycle which might be met in a part such as an aircraft wing which is exposed to periodic unpredictable load due to gusts.

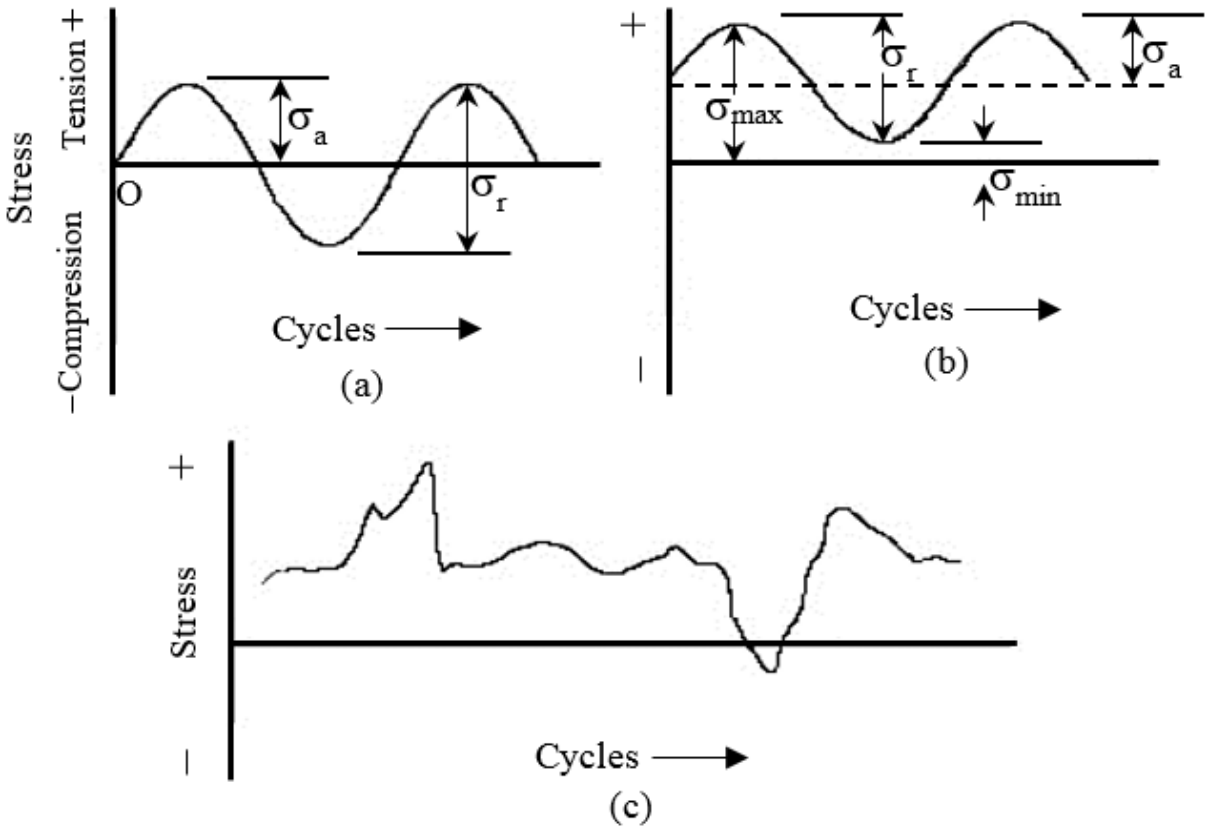

Fig. 2.3: (a) Reversed stress cycle (b) Repeated stress cycle (c) Irregular or random stress cycle.

2.5 Fatigue Cycling-Different extents

Fatigue failures can be classified into two forms encircling the total life of a component, namely low cycle fatigue (LCF) and high cycle fatigue (HCF). When $N < 10^4$ or 10^5 cycles is taken into account type of failure can be considered as LCF as well as when $N \geq 10^5$, as HCF. But the number of the cycles to failure is not more than 100 is come in the sub categories of very low cycle fatigue (VLCF) and if the fatigue failure takes place at a long span of time above 10^7 cycles than it said to be very high cycle (VHCF).

2.5.1 High Cycle Fatigue

The life of high cycle fatigue is generally considered as a function of applied stress range. After a number of cycles (typically more than 10^6 cycles) at comparatively low stress (typically less than 30 % of the yield stress) as well as the distortion experienced is primarily elastic in nature. When design part is subjected in the area of automobiles aircrafts, compressors, turbines, pumps etc. Where the chance of vibration is applicable than high cycle fatigue aspects must be counted for getting the better service life of such components. During HCF test, frequency is kept always more than 1 KHz. The S-N curve is usually referred in the state of high cycle fatigue as shown the schematic plot in Fig.2.4, where in the plot, S denotes the magnitude of cyclic stress and N indicates the cycles to failure; and the S Vs N plot is drawn in logarithmic scale.

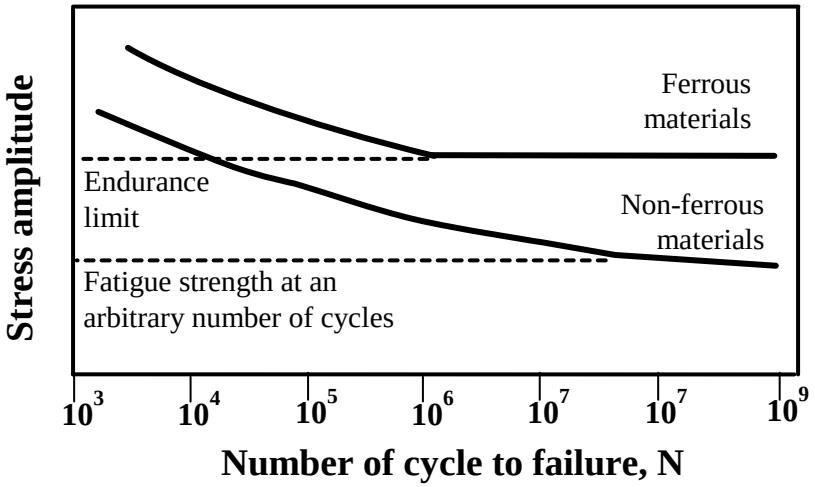

Fig. 2.4: Schematic repesentation of the S-N curve.

The above plot depicts as the number of cycle increases, the possibility of material failure increses with decresing stress. A few ferrous materials such as steel and titanium, the S-N curve converts horizontal after at a definite stress point. This stress point is known as fatigue limit or endurance limit where the material can tolerate an infinite number of cycles without rupture. Another gradually decreasing slope of non-ferrous materials like aluminium, copper and magnesium alloys with increasing number of cycles. These material never provide the actual endurance limit because curve never develops a horizontal line [22].

The S-N curve can be defined by Basquin equation:

$$N\sigma_a^p = C \quad \textbf{(2.1)}$$

Where,

N = number of cycles to failure

σ_a = stress amplitude

P and C are constants.

2.5.2 Very High Cycle Fatigue

During the very high cycle fatigue (VHCF), cyclic loading studies pointed out on the basis of the materials behavior, where the number of cycles to occur failure is more than $10^7$for high strength materials. It is very essential in order to design the components according to its critical and wide range of applications. It has been seen that in VHCF regime, cracks initiate from the interior portion of the specimen [25]. Failure due to fatigue occurs at stress levels less than conventional fatigue limit in long life regime more than 10^7cycles. A step by step S-N curve is shown in Fig. 2.6, where it clearly shown that in the portion C inhomogeneities of internal initiation with increasing inhomogeneities size and in portion D volume of fatigue strength remain constant till fatigue damage. The features of crack initiation and its near the beginning growth all are essential points to understand the VHCF nature. In both the conditions low cycle as well as high cycle fatigue, as we are very familiar that cracks begins owing to localized plastic deformation from the specimen external surface while in VHCF cracks tend to originate at interior sub-surface of the specimen. However, it often seen the effect of VHCF in various mechanical structures used for a long span of period such as automobiles, ships, aircrafts, railway, space equipments, bridges, off-shore structures and many more machineries components. To measure the VCHF aspects by the help of a single measurement which is a conventional type 20 Hz servo-hydraulic machine in the range of 10^9 cycles may take more than sixteen years. But recent techniques reduced the time to less than one week by using a 20 kHz ultrasound fatigue machine [26].

2.5.3 Low Cycle Fatigue

Generally, when stress is great enough for the plastic deformation to happen, the explanation of fatigue behavior in terms of stress value is almost less useful and a minor description is offered by strain in the material. In LCF, where the life is supposedly categorized as a function of the strain range and the failure comes in the material after a small number of cycles at a high stress, and the large plastic deformation take place. A component contracts as well as expands in response to fluctuations in operating temperature is happened in the thermal cycling by strain controlled cyclic loading. The low cycle fatigue is usually presented in the plot of strain range Δεp against number of cycles to failure (N). The plot is represented in log- log coordinates as shown in Fig.2.5, and the nature is described by Coffin-Manson relation:

$$\frac{\Delta\varepsilon_{\mathrm{p}}}{2} = \varepsilon_{\mathrm{f}}'(2\mathrm{N})^{\mathrm{c}'} \qquad \textbf{(2.2)}$$

Where,

$\Delta\varepsilon_{\mathrm{p}}/2 =$ the plastic strain amplitude,

2N= number strain reversals to failure (N cycles)

$\varepsilon_{\mathrm{f}}' =$ fatigue ductility coefficient or an empirical constant, the failure strain for a single reversal,

$\mathrm{c}' =$ fatigue ductility constant exponent or an empirical constant, varies from -0.5 and -0.7 for few metals.

The concept of low cycle fatigue is usually applied in designing the industrial components such as steam turbines, pressure vessels and other various kinds of machineries parts. In designing also the various structures, where seismic loadings are habitually applied. It has been reported by Pyttel *et al.* [27] and Shiozawa *et al.* [28] that a step by step or a dual S-N curve occurs for various materials, which was tested by the aid of rotary bending fatigue, clearly shown in Fig. 2.6.

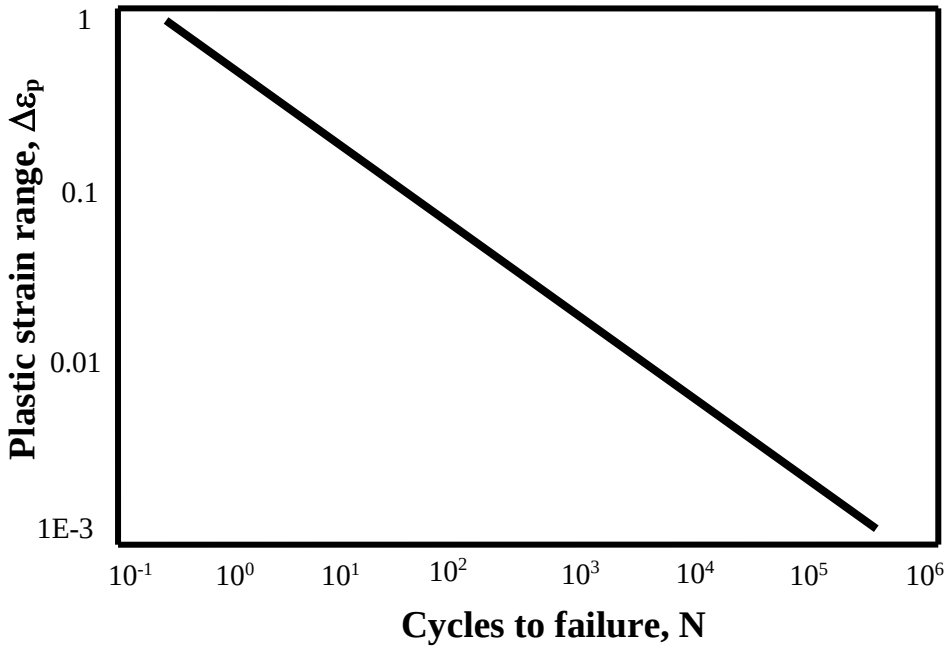

Fig.2.5: A schematic plot of plastic strain range against number cycles to failure. **(**$\Delta\varepsilon_p$ vs. N).

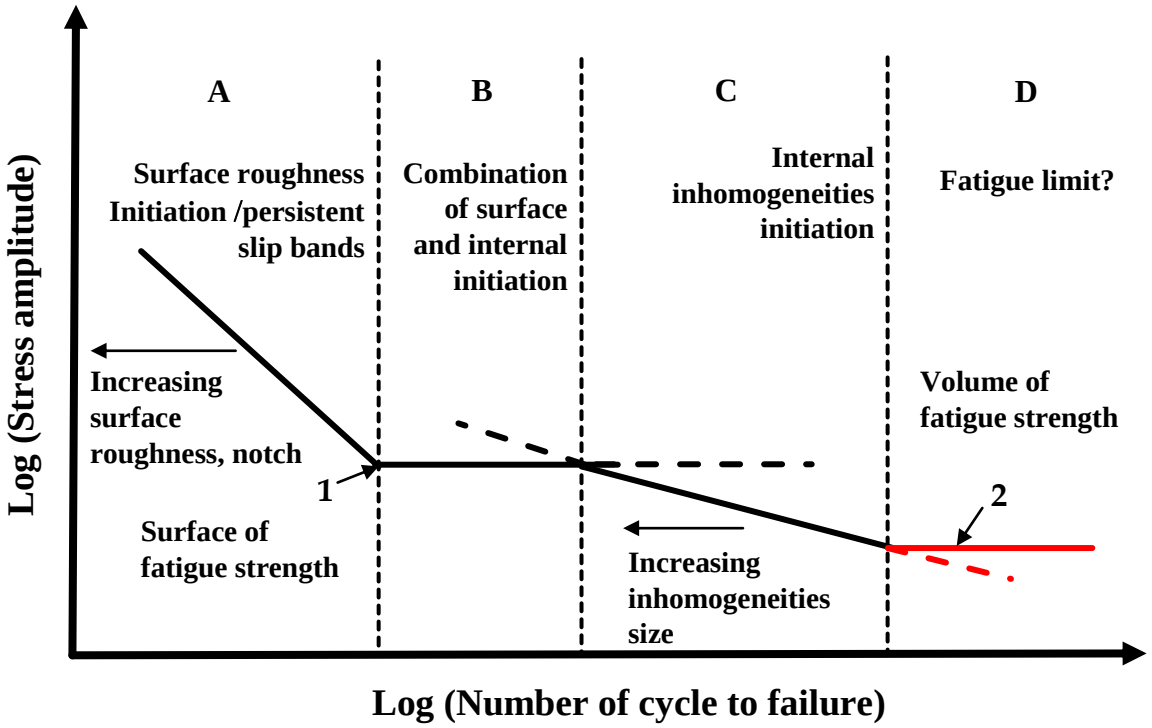

Fig. 2.6. Dual mode S-N curve with crack initiation sites.

2.5.4 Very Low Cycle Fatigue

During the very low cycle fatigue (VLCF), cyclic loading studies made on the behavior of the materials, where the number of cycles to failure is less than 100. It is very essential in order to design the components according to its applications. The major applications of it's in the field of rocket components designing and their life prediction, where the components subjected to high overloads, earthquakes and accidents etc. and to judge the amount of damage occurred during severe conditions of loading [29]. The fatigue loading can be taken either stress controlled mode or strain controlled mode during the experiment. In stress controlled loading.

2.6 Literatures available related to sensitization of stainless steel

Ghosh *et al.* [30] studied deterioration in fracture toughness of 304LN austenitic stainless steel due to sensitization. They found that the magnitude of degree of sensitization increases with the increasing time of sensitization for 304LN stainless steel. The slope for the degree of sensitization curve initially rises sharply and after certain period of time the gradient increases very slowly. The fall of ductility is found around 30% of the 100 hours sensitized stainless steel in comparison to its solution annealed condition. Instead of this deterioration in ductility, there is a small decrease in yield strength and hardness, whereas the tensile strength remains almost constant.

Jones and Randle [31] a splendid discussion made by them in sensitization behaviour of grain boundary engineered austenitic stainless steel. They told that austenitic stainless steels have a good combination of mechanical properties and exceptional corrosion resistance through a great temperature range due to these applications are extensive. The formation of chromium layer is the evidence of corrosion resistance. In the temperature range from 723 to 1173 K when a material hold for the periods of 1 to 100 of hours then chromium rich carbides leads to precipitate at grain boundaries and this depletion of chromium near the grain boundary is the sensitization. Contact to aggressive environments in a sensitised condition may turn to a breakdown in passivity and ensuing intergranular degradation as well as intergranular corrosion (IGC) and intergranular stress corrosion cracking (IGSCC) [32-34]. Sensitised grain boundaries provide linked networks for degradation. The morphology of carbide precipitation and subsequent sensitisation is shown which depend on grain boundary

structure. The arena of grain boundary engineering (GBE) has been developed over the last two decades pointing to advance intergranular properties in fcc materials through the growth of special grain boundaries [35-37]. In order to improve the resistance to sensitisation, IGC, IGSCC, and weld deterioration in austenitic stainless steels, GBE has been presented. They found that the degree of sensitization achieved by the heat treatment at 923 K decreases with increase in boundary length fraction. Increasing the fraction of boundaries through GBE process with a moderate grain growth provides an effective route of protection the subsequent degradation (i.e. sensitization and IGC).

Devine, T.M. [8] studied that the mechanism of sensitization austenitic stainless steel, where he focused the amount of chromium concentration not only along the grain boundaries, also normal to it. He calculated the amount of chromium depletion with the help of several models. He found that the variation in the amount of chromium carbide precipitation from grain boundary to grain boundary was considerable up to the 100 hours aging time. The precipitation of a high density of carbides along a large portion of the grain boundaries caused by sensitization after 100 hours hold time at 873 K.

2.7 Some pertinent literatures on low cycle fatigue of stainless steel

Ray *et al.* [38] studied that fatigue damage of AISI 304 LN stainless steel. They have been carried out a series of fatigue experiments on 304LN stainless steel keeping stress control mode and made their experiment simultaneously with a number of combinations of mean stress and stress amplitude. The behavior of cyclic loading of various structural components is generally treated by LCF, HCF and FCGR. In recent problems associated to LCF, the influence of symmetric ($\sigma_m = 0$) as well as asymmetric ($\sigma_m \neq 0$) loading situations. A lot of information associated to this discipline offers strain accumulation behavior under axial (i.e. uniaxial or multiaxial) loading states for cyclic hardening and softening of materials. They found that the amount of strain accumulation in selected steel increases with increase in the magnitude of peak stress of the executed cyclic loading, when the magnitude of mean stress is kept constant at preselected maximum values of stress encountered in a cycle. The amount of strain accumulation is found to be negligible under symmetric loading but it is considerable under asymmetrical loading whether the mean stress is positive or negative.

When the magnitude of mean stress is retained constant, the amplitude of alternating stress increases with decreasing the number of cycles to occur fatigue failure.

Ye *et al*. [39] investigated that the low-cycle fatigue deformation and final fracture of an austenitic stainless steel, where they were dealt about the low cycle fatigue characteristic of 304 grades of stainless steel, and it has been explained for many decades, despite that some little information added in this article on the LCF behavior of SUS304-HP stainless steel. It has been designated that nitrogen as an alloy element which has the capability to enhance the cyclic softening at low strain amplitude while it causes cyclic hardening at high strain amplitude. Nitrogen is the candidate element and addition of this in austenitic stainless steel increases the low cycle fatigue life as well as plays an important role in making the austenite stable. Addition of nitrogen as an interstitial element supports the stacking faults formation and also martensite during straining, which minimizes the crack growth and go ahead to rapid hardening (i.e. avoidance of plastic flow). The amount of martensite present, grain size, and strain amplitude decides the life of LCF. It has also been indicated whether the crack initiation or propagation, controlled fatigue life at a selected strain amplitude. The properties of LCF deteriorated due to the formation of martensite.

2.8 Some pertinent literatures associated with the estimation of dislocation density of stainless steel

Ungár [40] studied that dislocation densities, arrangements and character from X-ray diffraction experiments. Dislocations are a very habitual characteristic in crystalline materials and always present in both metals as well as alloys. These possess a wide variety of appearance, to keep an eye on their properties and presence a number of experimental techniques are available. X-ray techniques have made marvellous progress owing to their high resolution and synchrotron sources facilitating in order to measure diffraction profile peaks with great precision since last two decades. A variety of dislocation structures: (a) low density misfit dislocations in multilayers and thin films, (b) dislocation clusters in low quality layered structures, (c) special dislocations structures in intermetallic alloys exposing planar glide, (d) interface dislocations in heterogeneous microstructures and (e) chaotically distributed dislocations in bulk materials. All sources of X-ray diffraction techniques to estimate the dislocation densities from 100 to 10^{18} m^{-2} are accessible. Due to the heterogeneity of the microstructures, X-ray diffraction methods have exposed interface

dislocations. The examination of dislocations and Burgers vector study by Transmission electron microscope is more or less regular up to 10^{14} m^{-2} confined densities. A huge number of nondirect techniques such as XRD, neutron diffraction, magnetic Barkhausen noise, texture analysis ,convergent beam electron diffraction, small angle scattering, back scattering diffraction or electrical resistivity which gives a helpful information of different physical properties of materials.

Renzetti *et al.* [41] studied that X-ray evaluation of dislocation density in ODS-Eurofer steel. The dislocation density in metals can vary during plastic straining, phase transformation like martensitic transformation or thermal annealing. The quantitative assessment of dislocation density in metals is the key for the development of plastic theories of deformation. By using X-ray diffraction peaks and their broadening analysis, modified Williamson-Hall and Warren-Averbach methods were applied to calculate the dislocation densities. They found that the dislocation density of 80% cold rolled samples is 8×10^{15} m^{-2}. The values of dislocation density found in specimens annealed at 1100 °C and 1350 °C for 1 hour followed by air cooling are 7×10^{15} and 5×10^{15} m^{-2} respectively.

Chapter 3

Experimental Procedure

Outl i ne

Introduction

Material selection

Chemical composition

Heat treatment

Metallography

Optical microscopy

Grain size measurement

Hardness determination

Microhardness

Macrohardness

Mechanical testing

Specimen design

Tensile properties determination

Fatigue properties of material

Post fatigue tensile tests

Fractography

X-ray diffraction analysis

Estimation of dislocation density

3.1 Introduction

The main goal of this investigation is to acquire the tensile behavior owing to cyclic loading of sensitized stainless steel. In order to accomplish these goals, all required experiments were led which are stated in this chapter. An outline of all the experiments comprises selection of material, estimation of chemical composition of the selected steel, heat treatment in order to impose the sensitization effect, microstructural observation, determination of tensile behavior of the steel, fracture surface studies of deformed specimens, determination of hardness properties, study of X-ray diffraction profiles, low cycle fatigue behavior and field emission scanning electron microscopy.

3.2 Material Selection

The investigated steel is a non-conventional special grade austenitic stainless steel which is designated as **X12CrMnNiN17-7-5** according to ISO/TR 15510:1997 [45] was chosen for this investigation. Commercially, selected material is pure in nature. Initially, the material was available in the form of rods and the diameter of each rod was 16 mm with length of 120 mm.

3.3 Chemical Composition

The estimation of chemical composition of the selected steel was carried out by using optical emission spectrometer (model: ARL 3460 Metals Analyser, Thermo Electron Corporation Limited, Switzerland). Two measurements were carried out by using optical emission spectroscopy (OES) for both qualitative and quantitative estimation of impurity elements present in the commercial austenitic stainless steel. The acquired chemical composition of the selected steel is shown in Table 4.1.

3.4 Heat Treatment

The selected material was first procured from market, so idea about deformation present in it is unknown. So, it is essential to take out any residual stresses that may obtainable in it. The main motto of heat treatment is to soften the material, to alter the grain size, to change the structure of the material and to relieve the stress set up in the material subsequently either by hot working or cold working. Additional, heat treatment of austenitic stainless steel encompasses solution annealing, which aids in dissolving any precipitated carbide phase at high temperature. The precipitation of carbides may cause minor corrosion resistance.

Heat treatment process of the selected steel:

- ★ A few specimens were first solution treated by annealing at 1050^{o}C for 1 hour duration followed by water quenching.

- ★ To impose sensitization effect on the selected samples, heat treatment was carried out as per the schedule is given in the Table 4.2.

Table 3.1: Heat treatment of selected steel at different held time.

Sl.No.	No. of samples	Temperature, ^{o}C	Time, hrs.
1	2	750	1
2	2	750	3
3	2	750	5
4	2	750	7

All the samples were water quenched of duration stated.

3.5 Metallography

To examine the microstructure, samples of small size (i.e.10-15mm height) were cut from the solution annealed and sensitized condition rods separately. At the very first samples were grinded by using rough or non-precision grinding machine where the work is held in the operator's hand and pressed hard against the wheel, or vice-versa. Again samples were coarsely grinded by the aid of belt grinder by moving it up and back surfaces across the smooth file simultaneously, samples were kept cool by repeated dropping of water over it during the grinding operation. Grinding was done both the side of the samples to flatten the surface and was continued in anticipation of surface is flat, free from nicks, burr etc. After grinding, samples were polished by series of emery papers possessing consecutively finer abrasive. Emery papers of different grades 1/0, 2/0, 3/0 and at last 4/0 was used one by one during polishing. The specimens were moved in perpendicular direction to the existing scratches during all grinding and polishing operations.

After this, the closer and final approximation in order to make scratch-free, nicks or inflection free was done by the aid of wet rotating wheel covered with special cloth that was charged

with carefully sized abrasive particles.

After fine polishing, specimens were carefully washed with soap solution, and then dried using air drier. Polishing of these samples was accomplished using diamond paste up to 0.25 μm surface finish. In addition to that, the samples were electro polished in ice cooled atmosphere by using a solution of 80% acetic acid and 20% perchloric acid. To reveal the microstructure, polished specimens were etched with the freshly prepared aqua-regia solution [compose of 75%HCl and 25% HNO3]. Samples were kept indesiccators to avoid the direct contamination of open atmosphere.

3.5.1Optical Microscopy

Microstructures of the investigated samples were snapped by using optical microscope (model: Carl Zeiss Scope.A1 with AxioCam ERc5s, Germany), and images were taken at different magnifications. Optical microscope has been shown in Fig. 3.1.

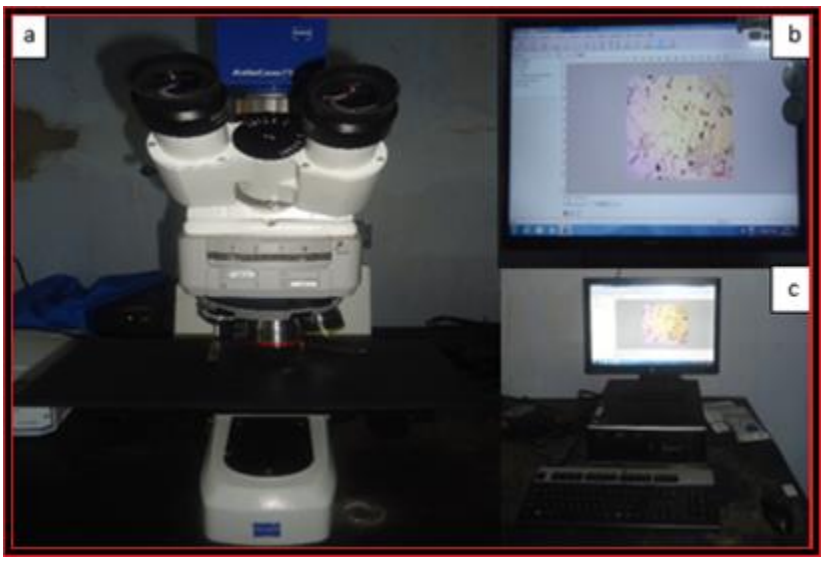

Fig. 3.1: Image of optical microscope.

3.5.2 Grain size Measurement

Determination of the average grain size of the investigated steel was done with the support of liner intercept method according to ASTM standard E-112 [46]. According to the method used here, a liner test grid was superimposed on the individual microstructures. Number of grains intercepted by the test lines was counted carefully. Such kind of measurements was

made at least 10 times on chosen fields at a magnification of 500X. The average grain size was estimated by using the belowmentioned formula:

$$d = \frac{L_T}{N_L} \quad \textbf{(3.1)}$$

Where,

N_L = number of grains intercepted by a unit true test line length.

L_T = true length of the test line.

True length of the test line can be defined as the length of the test line at unit magnification.

3.6 Hardness Determination

3.6.1Micro Hardness

Hardness tests were taken by using a Vickers Micro hardness Tester (model: Leco® LM248AT, USA) which is shown in Fig. 3.2. To make assure the accuracy of measurement, the opposite surfaces of these specimens were flatten and parallel by using belt grinder, followed by polishing of the specimens following the procedures already mentioned above prior to the tests.

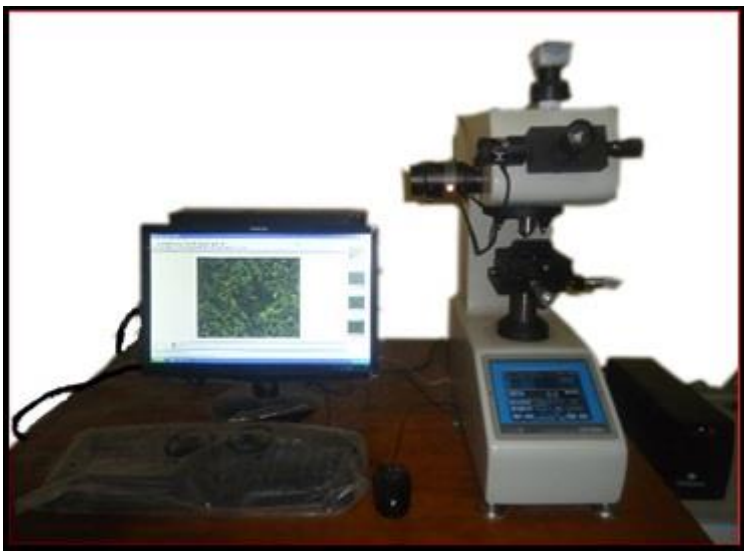

Fig. 3.2: Image of Leco®LM 248AT microhardness tester.

The polished surface of each specimen was indented at different locations. The load of 50gf and dwell time of 15 seconds was kept during these indentations on each of the samples. Five readings were taken on each sample in order to evaluate the average hardness value.

Vickers hardness was obtained by using the relations:

$$HV = \frac{1.854P}{(d_{avg})^2} \quad \textbf{(3.2)}$$

Where,

P= applied load in kgf.

$d_{avg} = (d_1 + d_2)/2$

Where, d_1 and d_2 are the length of indentation diagonals.

3.5.3.2 Macro Hardness

The macrohardness of the selected specimens were examined by the aid of Vickers macrohardness tester as shown in Fig.3.3. The indentations were made for each specimen at different locations. During these indentations load of 10 Kgf and dwell time 10 sec were kept. Five readings were recorded on each specimen to get the average value of hardness.

The hardness values were calculated by using the formula:

$$DPH = \left(\frac{1.854P}{L^2} \right) \quad \textbf{(3.3)}$$

Where,

P= applied load, Kgf

L= average length of indentation diagonals.

Fig.3.3: Image of Vickers macrohardness tester.

3.7Mechanical Testing

3.7.1 Specimen design fortensile and fatigue test

The specimens were fabricated from heat treated cylindrical rods of 120 mm initial length and 16 mm initial diameter according to ASTM standard E-8M-09[47]and the design of the specimens has shown in the Fig. 3.4. Cylindrical specimens 6 mm in diameter and 25 mm in gauge length were fabricated for tensile test and 6mm in diameter and 13 mm in gauge length for fatigue test. Specimens were polished in lathe machine up to fine polishing by using different grades of emery papers.

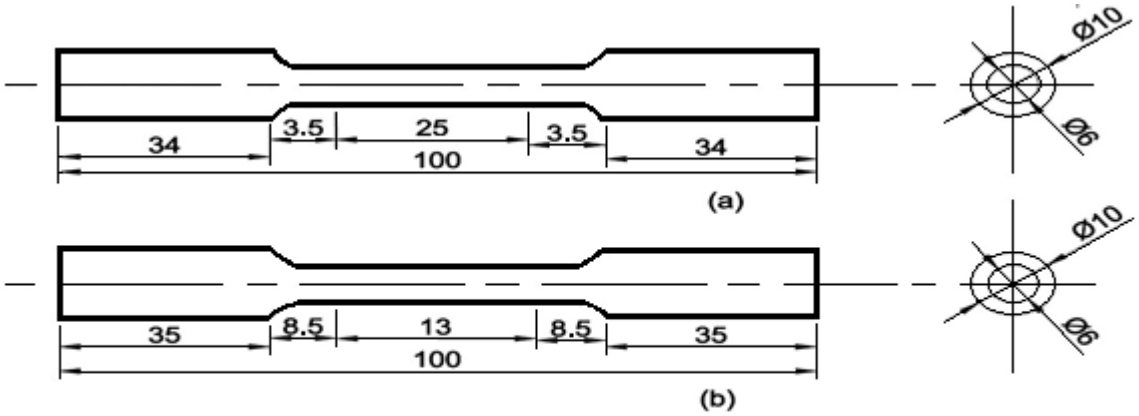

All dimensions are in mm

Fig. 3.4: Schematic configuration of (a) tensile specimen and (b) fatigue specimen.

3.7.2 Tensile properties determination

Tensile tests were conducted at ambient temperature (i.e. 300 K) by using BISS universal testing machine of capacity ±100 kN (model: BISS UTM, Bangalore, India) as shown in Fig.3.5, which was integrated with computer and operated by software MTL32. Test builder is the softwareof another kind which helps to maintain limitations to run the machine in safe mode. Prior to test, specimens gauge diameter and gauge length was noted down before and after the test. Tests were carried out at a constant cross head speed of 1 mm/min, which corresponds to insignificant strain rate of $6.66\times10^{-4}s^{-1}$. Load–displacement signals were generated automatically by the machine and the generated digital values of the same were stored in the computer in specified folder for further use.

3.7.3 Fatigue properties of material

Strain controlled low cycle fatigue tests were carried out at ambient temperature (i.e. 300 K) up to 100 cycles by using BISS universal testing machine of capacity ±100 kN (model: BISS UTM, Bangalore, India) as shown in Fig. 3.5. Prior to run the machine, settings were done in LCF programme. All specimens used for fatigue tests were similar kind to those used for tensile test, only with difference that the fatigue samples were of 13 mm gauge length. The tests were carried out at a strain rate of 4×10^{-3} s^{-1}. For each solution annealed as well as sensitized condition, three specimens were taken. The total strain amplitude of 0.25%, 0.50%, 0.60% were kept for every other specimens. The parameters that have been provided for this test is stress amplitude (σ_a) mean stress (σ_m) and number of cycles (N).

In order to calculate the value of frequency, below mentioned relation has been used:

$$\text{Frequency} = \left(\frac{4 \times \text{amplitude}}{d\varepsilon/dt} \right)^{-1} \quad \textbf{(3.4)}$$

Where,

$d\varepsilon/d_t$= Strain rate.

The obtained values of frequency were 0.40, 0.20 and 0.16 for strain amplitude of 0.0025 0.005 and 0.006 respectively, which were taken during LCF programme setting before starting the test.

Fig. 3.5: BISS universal testing machine capacityof ±100 kN.

3.7.4 Post fatigue tensile tests

After the accomplishment of strain controlled low cycle fatigue test, specimens were subjected to tensile test at a constant crosshead speed of 1 mm/min. This constant crosshead speed to agree to an insignificant strain rate of $6.66 \times 10^{-4} s^{-1}$. Load–displacement signals were generated automatically by the machine and the generated digital values of the same were stored in the computer in specified folder for further use.

3.8 Fractography

Fig.3.6: (a) Undeformed specimen and broken tensile specimens of (b) solution annealed (c) sensitized.

In order to investigate the fracture surface of broken tensile samples were cut out carefully of 1mm size within the gauge portion. Typical configurations of solution treated and one of sensitized specimens are shown in Fig.3.6. Fractographs of the fractured surfaces were recorded by using field emission scanning electron microscope (model: Nova NanoSEM 450) by FEI™ made in Czech Republic, Brno with electron dispersive spectroscope (EDS) from "BRUKER" (liquid nitrogen free) made in Germany. It consist "resolution" in high vacuum mode is 1nm at @15 kV with spot size 1and "magnification" upto 6 Lakhs (i.e. 600 kx). Images were captured at different magnifications. EDS analysis was also carried out in order to define the phases present in it. Field emission scanning electron microscope has been shown in Fig. 3.7. To identify the nature of fracture morphology, a series of representative fractographs were taken.

Fig. 3.7: Image of Nova NanoSEM 450 Field Emission Scanning Microscope.

3.9X-ray Diffraction Analysis

Generally, X-ray diffraction technique was used to classify the different type of phases (i.e. elemental phase/ intermetallic phase/crystalline phase/non-crystalline phase) present in the target sample. The XRD profiles were taken to determine the dislocation density of specimens were cut of 1 mm height and 10 mm diameter. Samples were subjected to X-ray diffractometer (model: XPert-3040Y00, Holland) high resolution Cu-Kα (λ=1.5418 Å) radiation at the target were carried out as shown in Fig. 3.8. Samples were exposed to generate X-ray diffraction with operating voltage of 30 kV in the scanning range of 32°-120° and at scan speed of 2°/min. Intensity peaks were analysed by the aid of Philips X'PertHighscore software.

Fig. 3.8: Image of X-ray diffraction analyser.

3.10Estimation of dislocation density

The modified Williamson-Hall equation [45] is used to estimate the dislocation densities: (a) as- received as well as sensitized specimens (b) deformed specimens of as-received and sensitized. The detailed calculation has been given in chapter 4.

Chapter 4

Results and Discussion

Outl i ne

Introduction

Chemical composition

Microstructural analyses

Grain size measurements and their distribution

Hardness determination

Tensile properties determination

Low cycle fatigue behavior

Post fatigue tensile Properties

Fractographic examinations

X-ray diffraction analyses

Estimation of dislocation density

4.1 Introduction

The aim of this research is to analyze the low cycle fatigue (LCF) behaviour and its effect on tensile behavior of a non- conventional austenitic stainless steel predominantly under sensitized condition. It was also intended to analyze the dislocation density of deformed specimens of sensitized stainless steel. In order to accomplish these aims a range of experiments have been carried out, which is explained with proper evidence of the work in the preceding chapter. This chapter contains the obtained results of all the individual experiments carried out for the duration of this investigation along with their pertinent discussion. This chapter is composed of various sub sections-**Section 4.2** deals in chemical composition of the non-conventional stainless steel; microstructural analyses for all conditions have been depicted in **Section 4.3**; grain size measurement and their distribution and hardness properties with relevant discussion have been provided in **Sections 4.4** to **4.5**; tensile properties results with their discussion have been discussed in **Section4.6**; low cycle fatigue damage and their effect on tensile properties have been represented with pertinent discussion in **Sections 4.7** to **4.8** and the last, the results of fractographic examinations, X-ray diffraction profile analyses, estimation of dislocation densities for the similar conditions have been stated in **Sections 4.9** to **4.11** respectively.

4.2 Chemical composition

The Chemical composition of the investigated steel was obtained by optical emission spectrometer (OES) as shown in Table 4.1, which indicates that steel possess a special grade of non-conventional stainless steel termed as X12CrMnNiN17-7-5. This grade of stainless steel is similar to X5CrNi17-7 [46]. X12CrMnNiN17-7-5 stainless steel owns good mechanical properties and superior corrosion resistance against degradation. This grade of steel are predominantly used for automotive parts such as automotive trim, automotive wheel covers and also use in flat conveyor chains, flatware, railroad passenger car bodies, structural members, architectural applications etc. It is well said that austenitic stainless steels contain major alloying elements as Cr and Ni around in the range of 16-25% and 8-20% respectively with low amount of carbon content [1].

The investigated stainless steelcontains 0.14% carbon with common alloying elements of Ni and Cr as 3.66% and 15.6% respectively. The steel also possess 5.49% Mn. Addition of

manganese make this special grade of steel enable to conserve Ni. As the alloying elements are different as compared to that in conventional 300 series austenitic stainless steel, this steel is referred to as non-conventional austenitic stainless steel [46]. It very fact that Ni, Mn and N are austenite stabilizers and hence this steel is austenitic at room temperature and the crystal structure of the steel is face centered cubic (fcc).

Table 4.1: Chemical composition of non-conventional stainless steel (all in wt. %).

Material	**Elements**						
ISO/TR 15510X12CrMnNiN17-7-5 SS	**C**	**Ni**	**Cr**	**Mn**	**Al**	**Ti**	**V**
	0.14	3.96	15.6	5.49	0.03	0.02	0.06
	Si	**S**	**P**	**Mo**	**Cu**	**N**	**Fe**
	0.53	0.016	0.042	0.2	1.05	0.135	Bal

4.3 Microstructural analyses

Optical microstructure of the investigated non-conventional stainless steel reveals that the steel possesses equiaxed austenite grains. A typical micrograph of the investigated solution annealed stainless steel is shown in Fig. 4.1 and the microstructures of the sensitized steel

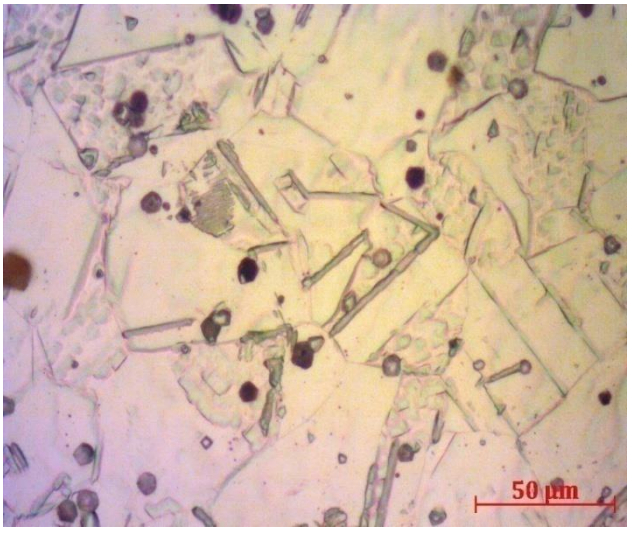

Fig.4.1: Microstructure of solution annealed non-conventional stainless steel.

Indicate that the volume fraction of the sensitized grain boundaries increases with an increasing time of sensitization as illustrated in Fig. 4.2.

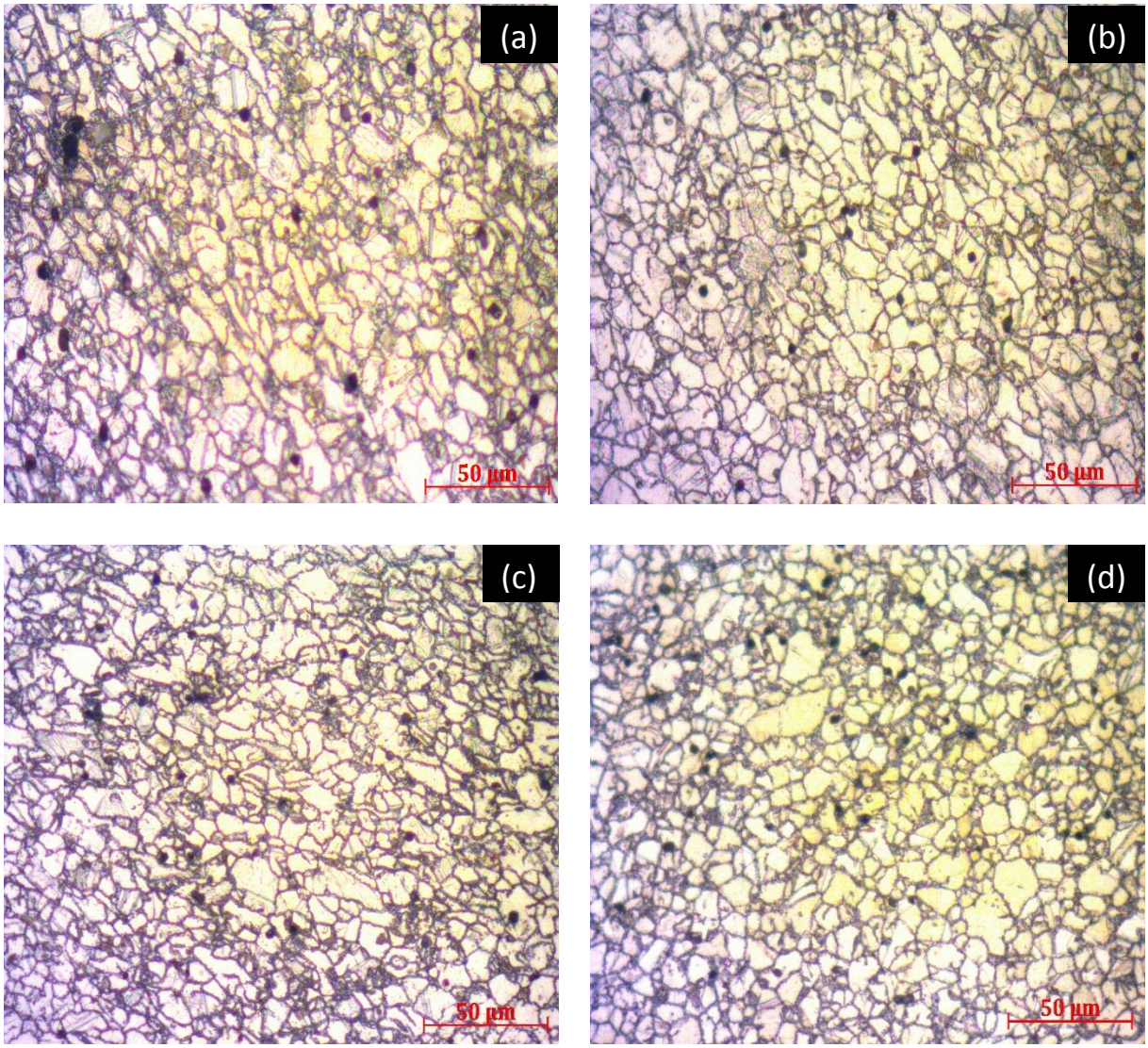

Fig.4.2: Microstructures of non-conventional stainless steel sensitized for (a) 1 hr, (b) 3 hrs, (c) 5 hrs, and (d) 7 hrs.

4.4 Grain size measurements and their distributions

The average grain size for all conditions was determined by using linear intercept method according to ASTM standard E112 [47] as given in Table 4.2. A liner test grid superimposed micrograph of solution annealed non-conventional stainless steel is shown in Fig.4.3 to witness the method. Linear intercepts were imposed on the microstructures separately at

magnification of 500X. Plots in Fig. 4.4 (a) – (e) illustrate the grain size distribution of annealed as well as sensitization stainless steel.

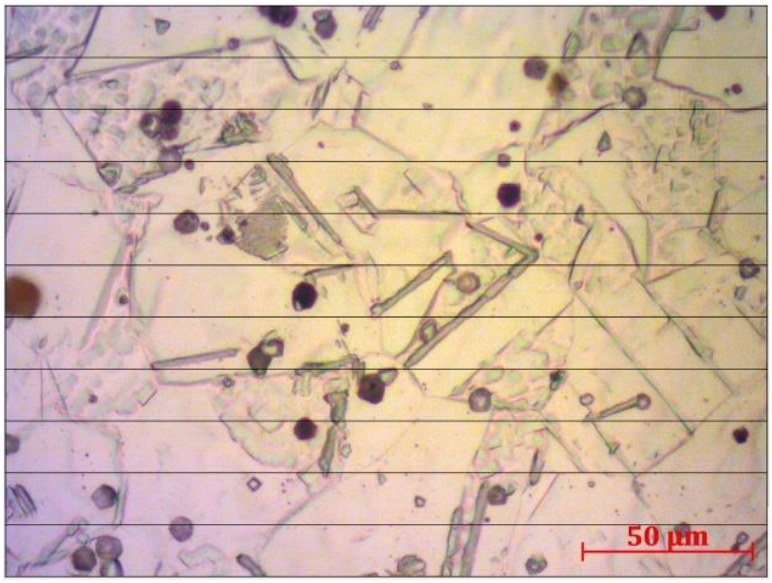

Fig.4.3: Superimposed liner test grid microstructure of solution annealed specimen.

Table 4.2: Average grain size of solution annealed and 1hr, 3hrs, 5hrs and 7 hrs sensitized specimens.

Sample condition	**Solution annealed**	**Sensitized**			
		1 hr	3 hrs	5 hrs	7 hrs
Avg. Grain size, µm	23.49±4.40	7.81±0.40	7.91±0.38	8.02±0.42	8.43±0.47

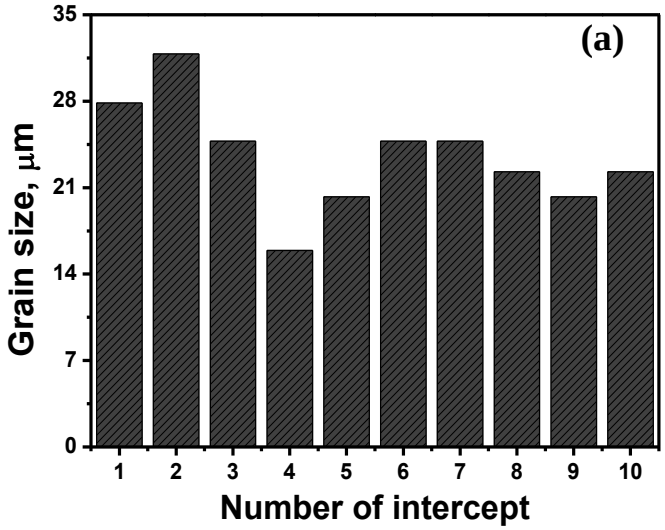

Fig. 4.4:(a) Grain size distribution of the solution annealed steel.

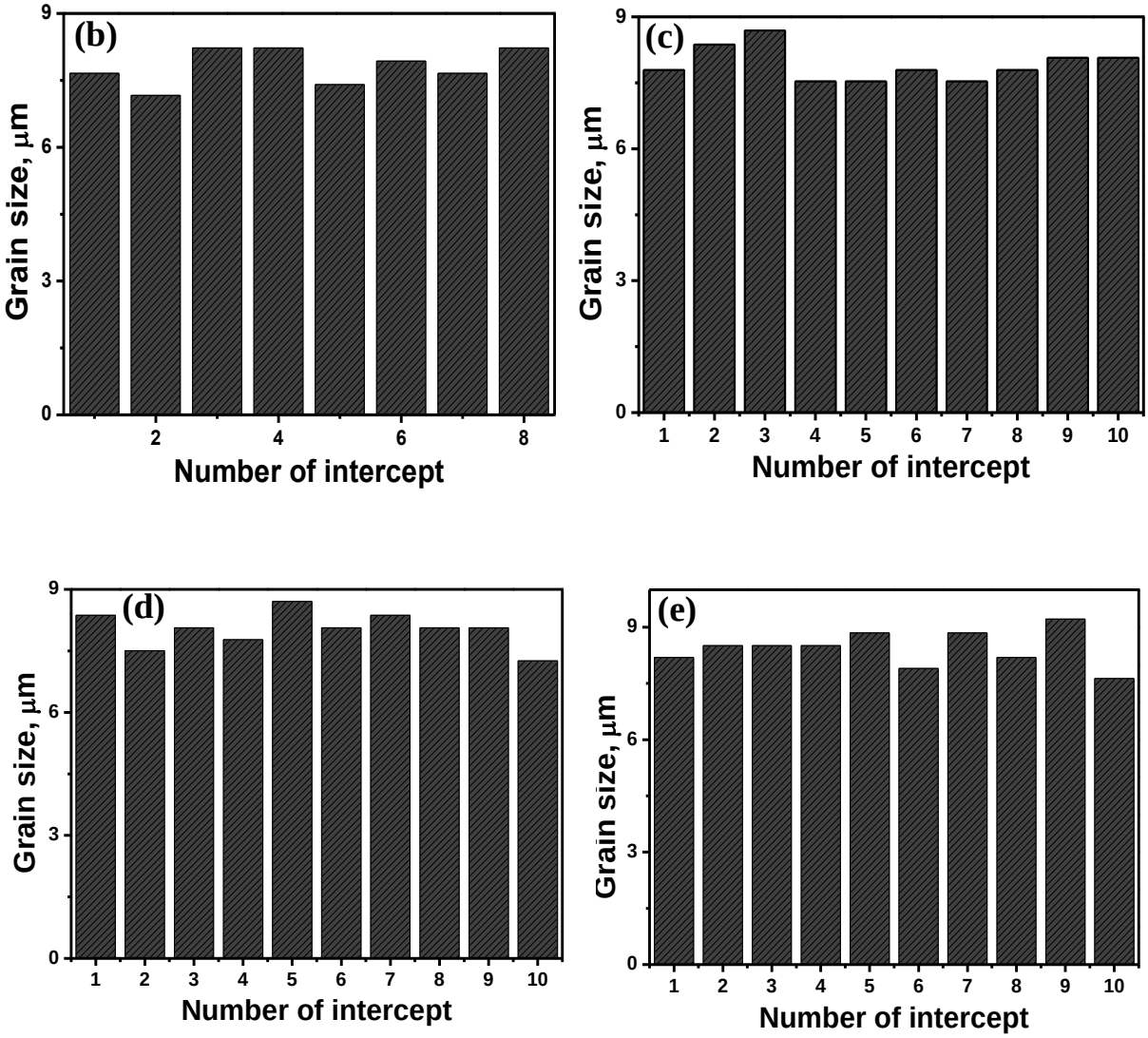

Contd.... Fig. 4.4: Grain size distribution of (b) 1 hr, (c) 3 hrs, (d) 5 hrs and (e) 7 hrs sensitized steels.

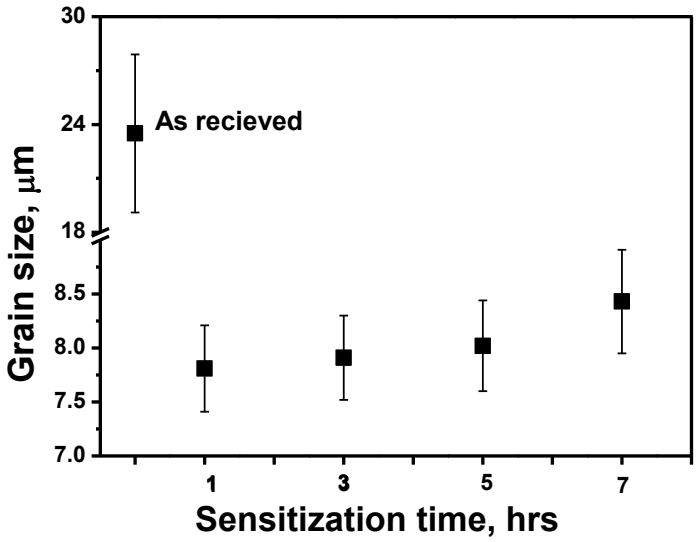

Fig. 4.5: Grain size distribution for all conditions.

It can be seen that in solution annealed conditions the grain sizes vary a lot whereas in sensitized condition this variation is less. The Standard deviation of all these variations is shown in Table 4.2 as well as Fig. 4.5.

4.5 Hardnessdetermination

Microhardness values of the non-conventional stainless steel have been taken at different positions of the sample. At least five readings have been taken for each sample to obtain average value of hardness.

Dwell time for microhardness test is 15 sec, with applied load of 50gf. As per literature, austenitic stainless steels possess hardness ≈ **200** VHN [50]. Type A^* indicate that the average hardness of the solution annealed sample is **200.48** Hv. From Table 4.3, it is clear that hardness of the investigated stainless steel falls under the hardness range of austenitic stainless steel. The result of all the samples is listed in Table 4.3.

Table 4.3: Microhardness values of the investigated steel.

Type	1st reading			2nd reading			3rd reading			4th reading			5th reading			Avg.
	D1, μm	D2, μm	HV	D1, μm	D2, μm	HV	D1, μm	D2, μm	HV	D1, μm	D2, μm	HV	D1, μm	D2, μm	HV	
A*	21.24	21.64	201.7	21.28	21.88	199.1	21.49	21.39	201.7	21.55	21.41	201	21.39	21.79	198.9	**200.48**
B*	18.11	17.39	294.3	18.14	17.22	296.6	18.22	17.29	294.1	18.02	17.78	289.4	18.31	17.35	291.7	**293.22**
C*	20.19	20.19	227.5	20.28	20.18	226.6	20.14	20.08	229.3	20.51	20.48	220.7	20.23	20.21	226.8	**226.18**
D*	19.39	18.48	258.6	19.27	19.23	250.2	19.21	19.18	251.7	19.34	19.27	248.8	19.38	19.32	247.6	**251.38**
E*	18.22	18.37	277	18.48	18.45	271.9	18.33	18.45	274.2	18.62	18.56	268.3	18.3	18.37	275.8	**273.44**

* A-Solution annealed, B-1 hr sensitization, C-3 hrs sensitization, D-5 hrs sensitization, E-7 hrs sensitization**.**

Ghosh *et al.*[30] reported that the hardness of sensitized stainless steel decreases as the time of sensitization increases. The reason behind it is explained as: during sensitization carbides form and thus there exists chromium depleted zone in the steel. This leads to the depletion of the solid solution strengtheners (C, Cr, N, Ni etc.) from the matrix, which results in softening of the matrix. Thus there is a decrease in the hardness. The variation of microhardness and macrohardness values are shown in Fig. 4.6 and Fig. 4.7 respectively. All the results of macrohardness tests are given in Table 4.4. It can be seen from Fig. 4.6 that, the curve does not follow any particular trend. This phenomenon occurs due to the fact that assessment of microhardness is done over very small area, such that a region near the grain boundary can show higher hardness. To avoid ambiguity, macrohardness studies have been done which show continuous fall in hardness values with sensitization time.

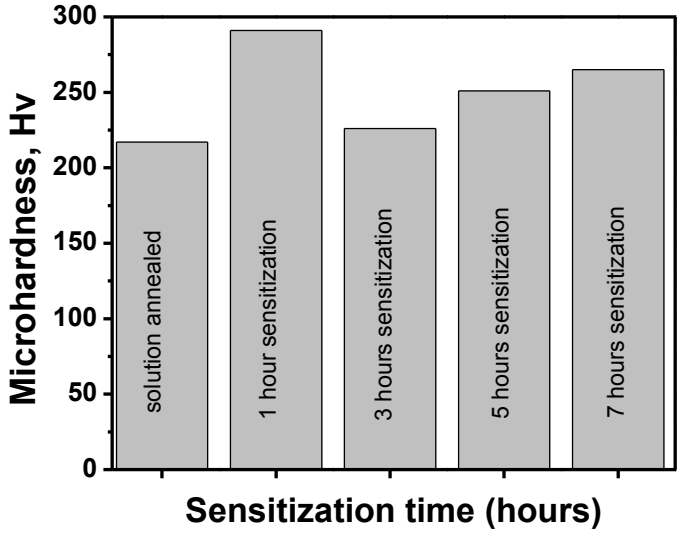

Fig. 4.6: Microhardness variation with sensitization time.

Table 4.4: Macrohardness values of the investigated steel.

Material Condition		Hardness					HV_{avg}	Standard deviation
		value 1	value 2	value 3	value 4	value 5		
Solution annealed		215	209	218	213	207	212.4	4.44
Sensitization time, hours	1	192	190	186	197	188	190.6	4.21
	3	184	193	188	182	190	187.4	4.44
	5	189	180	187	187	185	185.6	3.43
	7	187	184	182	179	185	183.4	3.04

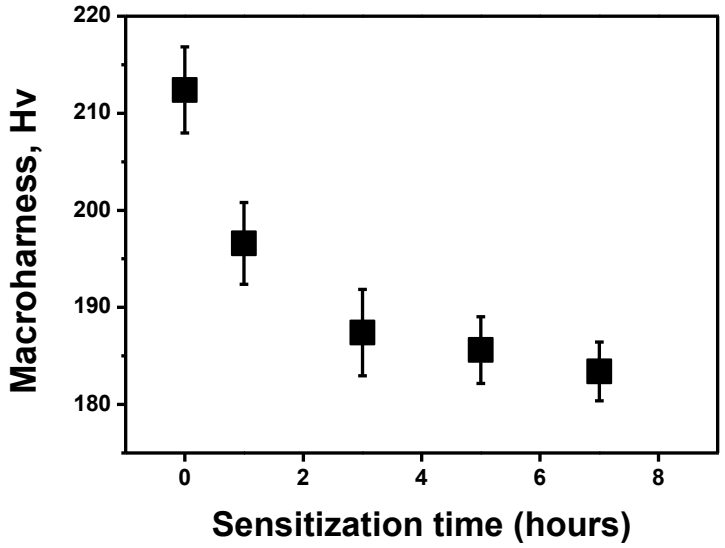

Fig. 4.7: A plot of macrohardness against the time of sensitization.

4.6 Tensile properties of stainless steel

To get the load and displacement values for both solution annealed as well as sensitized conditions, tests were conducted under the BISS universal testing machine at room temperature. Further, the calculations were made for the corresponding stress and strain values and the plot between stress-strain were depicted. Owing to lack of sharpness in yield point, yield points were determined by taking offset of 0.2% (or 0.002) according to ASTM standard E8M [48] for all the cases, where a straight line was drawn parallel to the initial linear portion of the curve on stress-strain plot. Fig. 4.8 (a) shows the engineering stress-strain curve of solution annealed stainless steel and that for (b) 1 hour, (c) 3 hours, (d) 5 hours, (e) 7 hours sensitized conditions obtained by doing tensile tests with a cross head speed of 1mm/min. This cross head speed corresponds to a nominal strain rate of 6.66×10^{-4}.

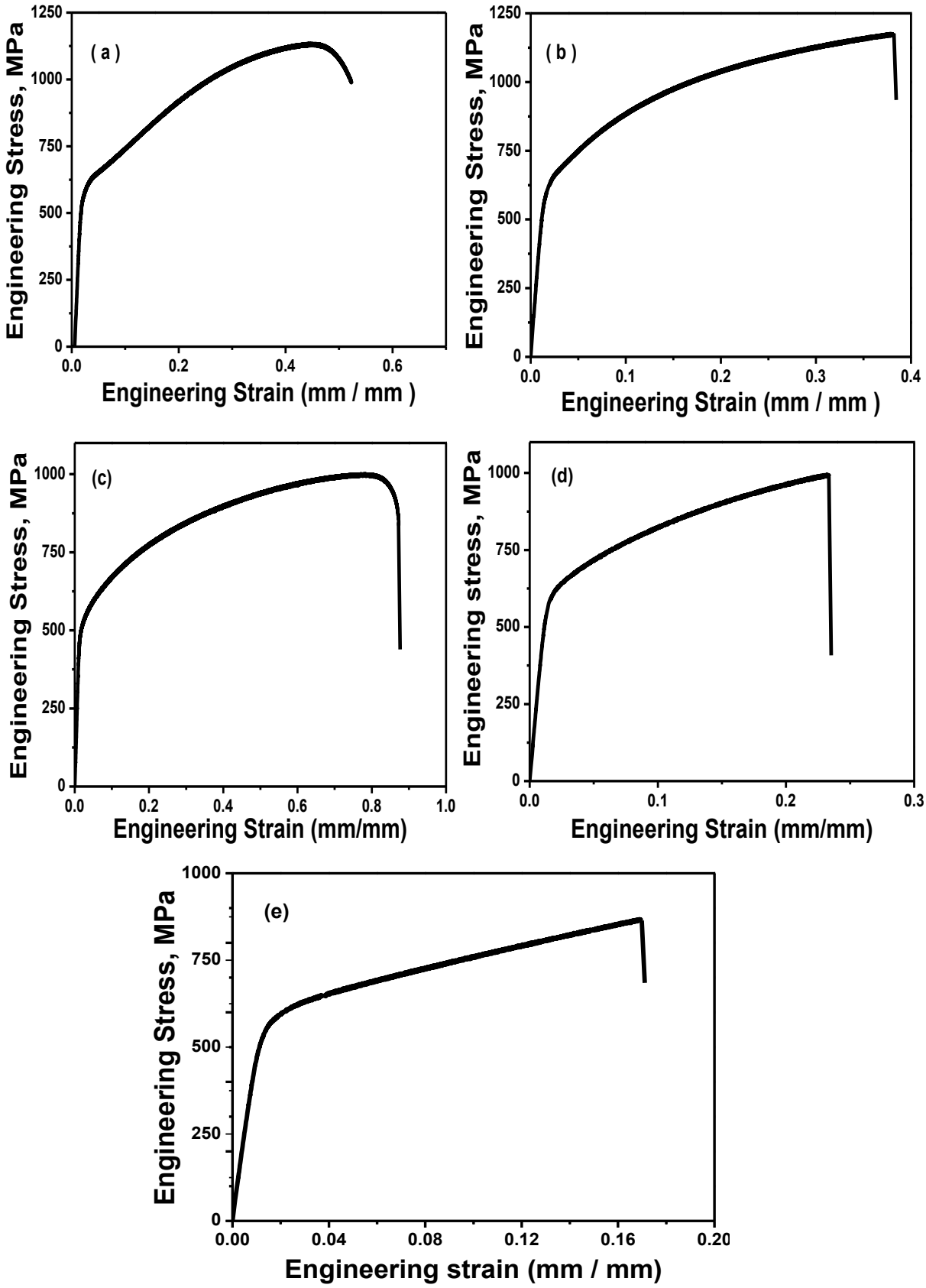

Fig.4.8: Engineering stress-strain plot of the selected stainless steel (a) solution annealed condition and (b) 1hour, (c) 3 hours, (d) 5 hours, (e) 7 hours sensitized conditions.

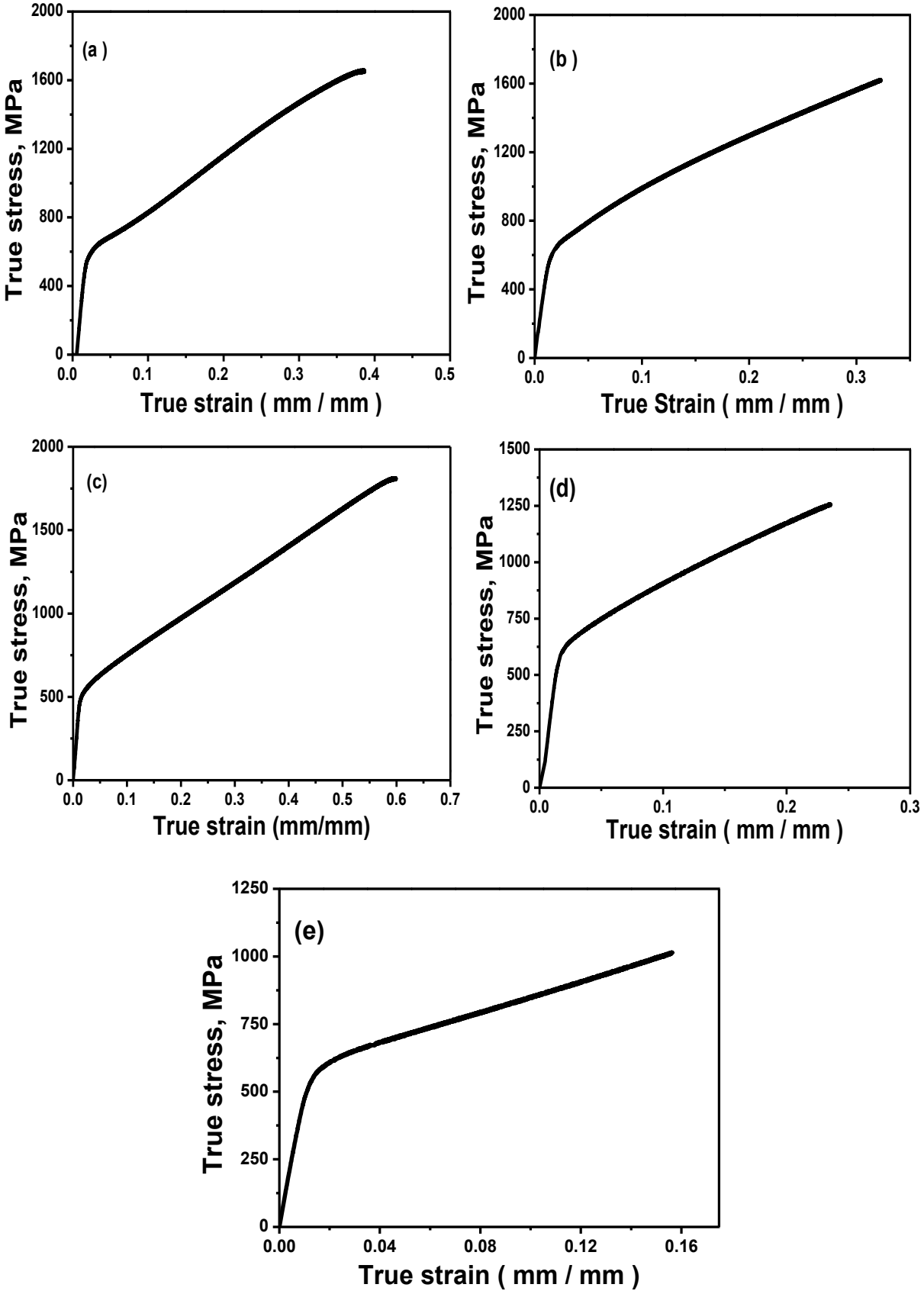

Fig.4.9: True stress-strain plot of the selected stainless steel (a) solution annealed condition and (b) 1hour, (c) 3 hours, (d) 5 hours, (e) 7 hours sensitized conditions.

Table 4.5: Tensile properties of the investigated non-conventional stainless steel.

Specimen condition	YS (MPa)	UTS (MPa)	% UE(ε_u)
Solution annealed	635	1174	44.83
1 hour sensitized	595	1133	37.81
3 hours sensitized	543	999	78.69
5 hours sensitized	524	994	23.00
7 hours sensitized	503	868	16.87

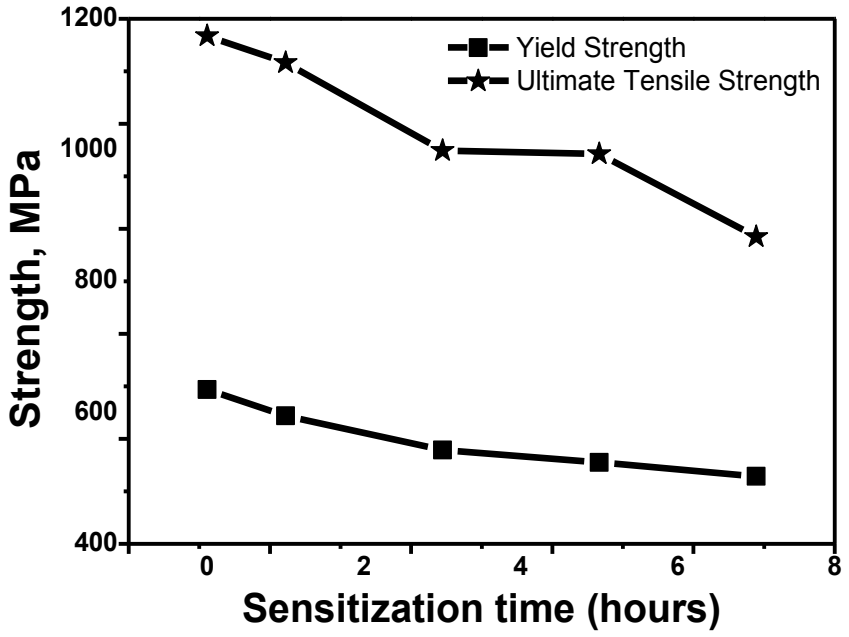

Fig. 4.10: Effect of sensitization time on Yield strength and Ultimate tensile strength.

4.7 Low cycle fatigue behaviour

The investigated non-conventional stainless steel has been studied in both solution annealed as well as sensitized conditions for their low cycle fatigue behavior under symmetrical strain cycling at room temperature with various strain amplitudes (i.e., 0.25%, 0.50% and 0.60%) for each set of specimens. The cyclic stress-strain hysteresis loops under uniaxial strain cycling are shown in Fig. 4.11 to Fig. 4.14 with different strain amplitudes. Moreover, the maximum and minimum stress values vs. 'number of cycles' plots are shown in Fig. 4.15 to Fig. 4.16. It can be seen from all the hysteresis loops presented here that the curves shift downward with increasing number of cycles. Fig. 4.11 is a typical representation of 1^{st}, 20^{th}, 50^{th} and 100^{th} cycle data for the investigated solution annealed sample for strain amplitude of 0.50%. These curves clearly show that required stress for producing same strain for each cycle is reducing.

A thorough insight to the stress vs. 'number of cycles' behaviour for the specimens indicate that the steel features cyclic hardening in the initial few cycles followed by which the cyclic softening takes place. One can note that the maximum stress reduces while minimum stress increases for the same strain amplitude after initial few cycles for almost all the cases. However, for the case of 7 hrs sensitized specimens (shown in Fig. 4.16d), cyclic hardening takes place for all the employed strain amplitudes. Additionally, it may be mentioned that for low strain amplitude, cyclic softening takes place after a few initial cycles of hardening. The initial hardening may be considered to occur by the influence of martensitic transformation in the steel; the structure of this grade of stainless steel is metastable in nature [49] and austenite transforms to martensite upon deformation. The employed strain amplitude is low, which causes non-remarkable extent of phase transformation. Martensitic transformation contributes to the increase the strength up to few cycles. At higher cycles, the cyclic softening feature gradually dominates over the process, than the hardening by martensitic transformation.

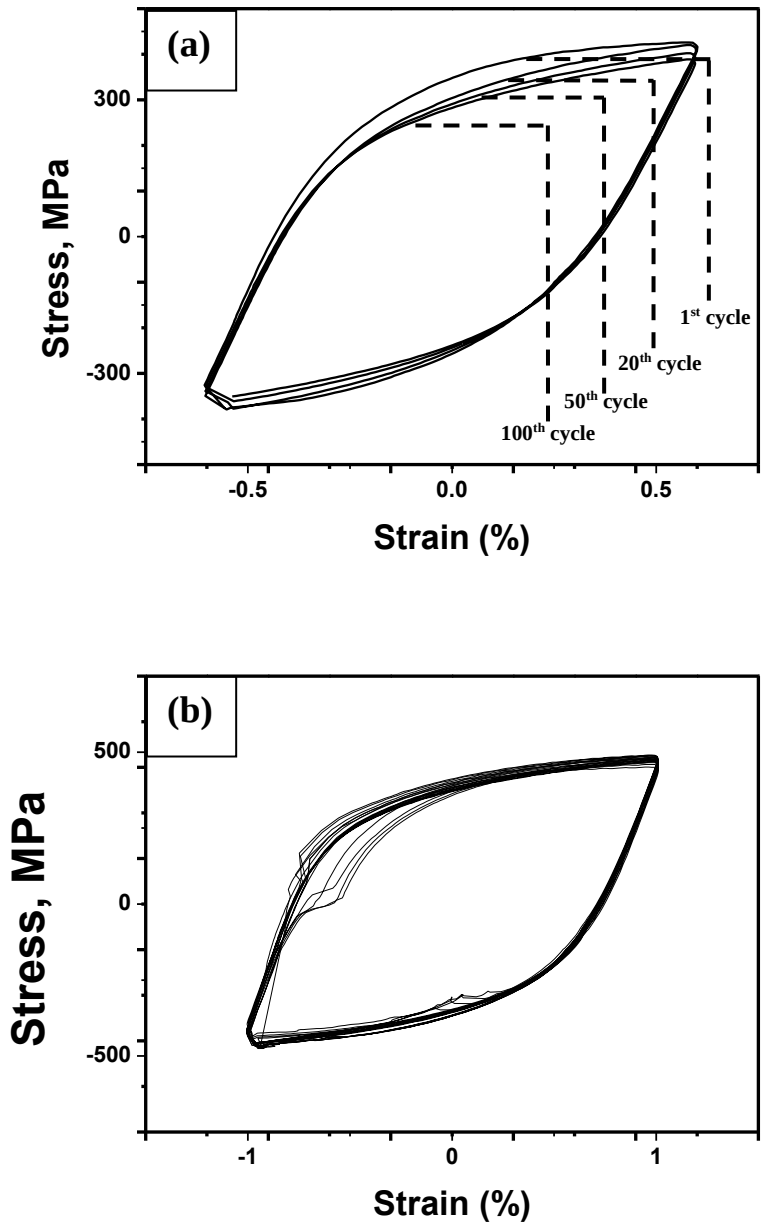

Fig. 4.11: Hysteresis loops generated during a LCF test at (a) stain amplitude (ε_t) of 0.50% and (b) stain amplitude (ε_t) of 0.60% for solution annealed case.

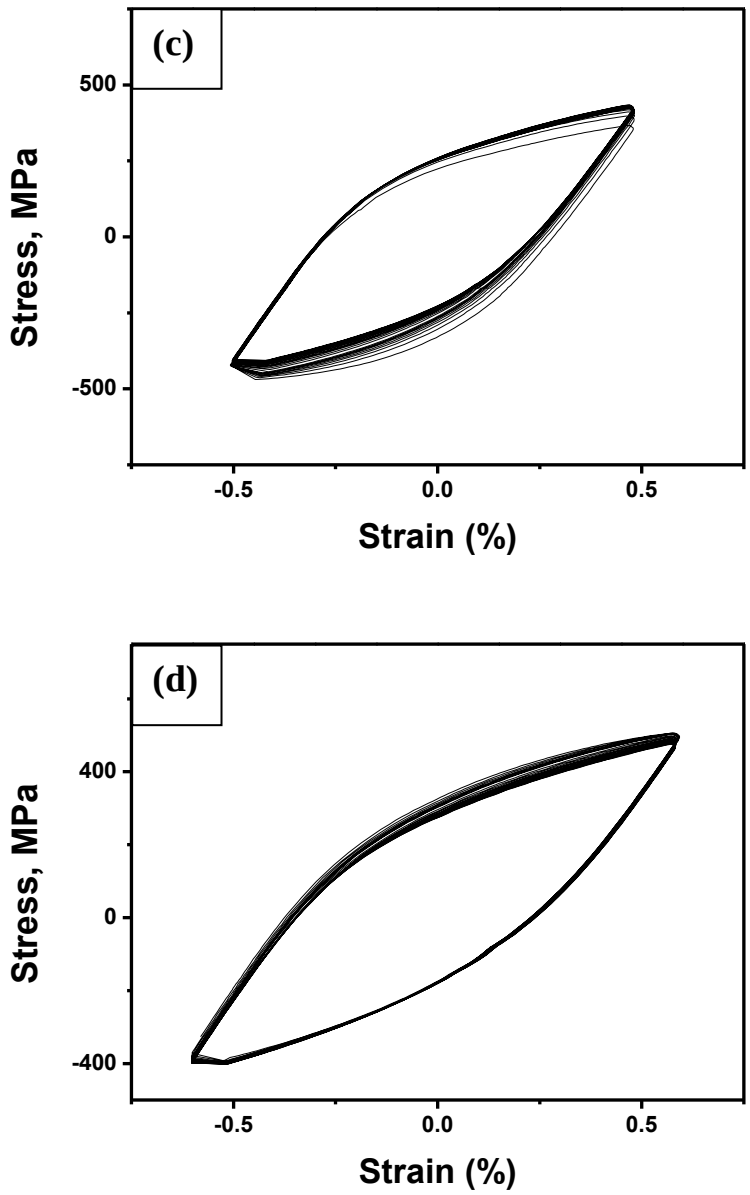

Fig. 4.12: Hysteresis loops generated during a LCF test at (c) stain amplitude (ε_t) of 0.50% and (d) stain amplitude (ε_t) of 0.60% for 3 hours sensitized case.

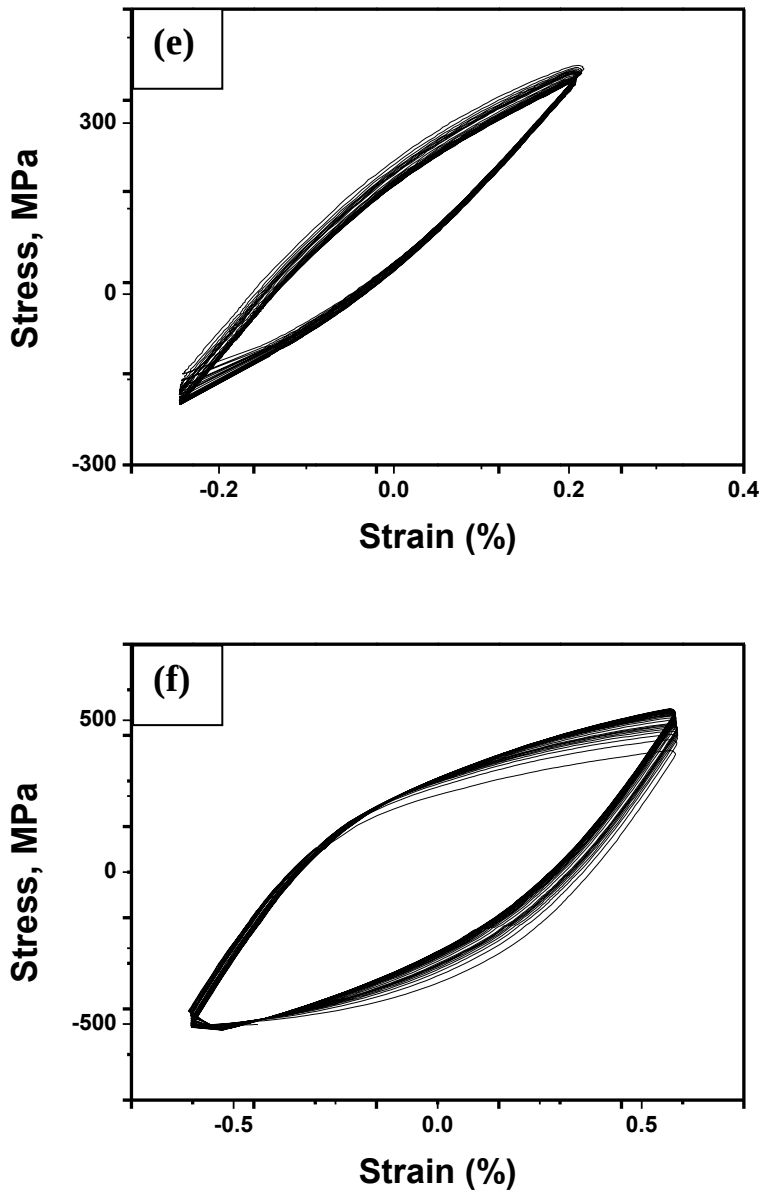

Fig. 4.13: Hysteresis loops generated during a LCF test at (e) stain amplitude (ε_t) of 0.25% and (f) stain amplitude (ε_t) of 0.60% for 5 hours sensitized case.

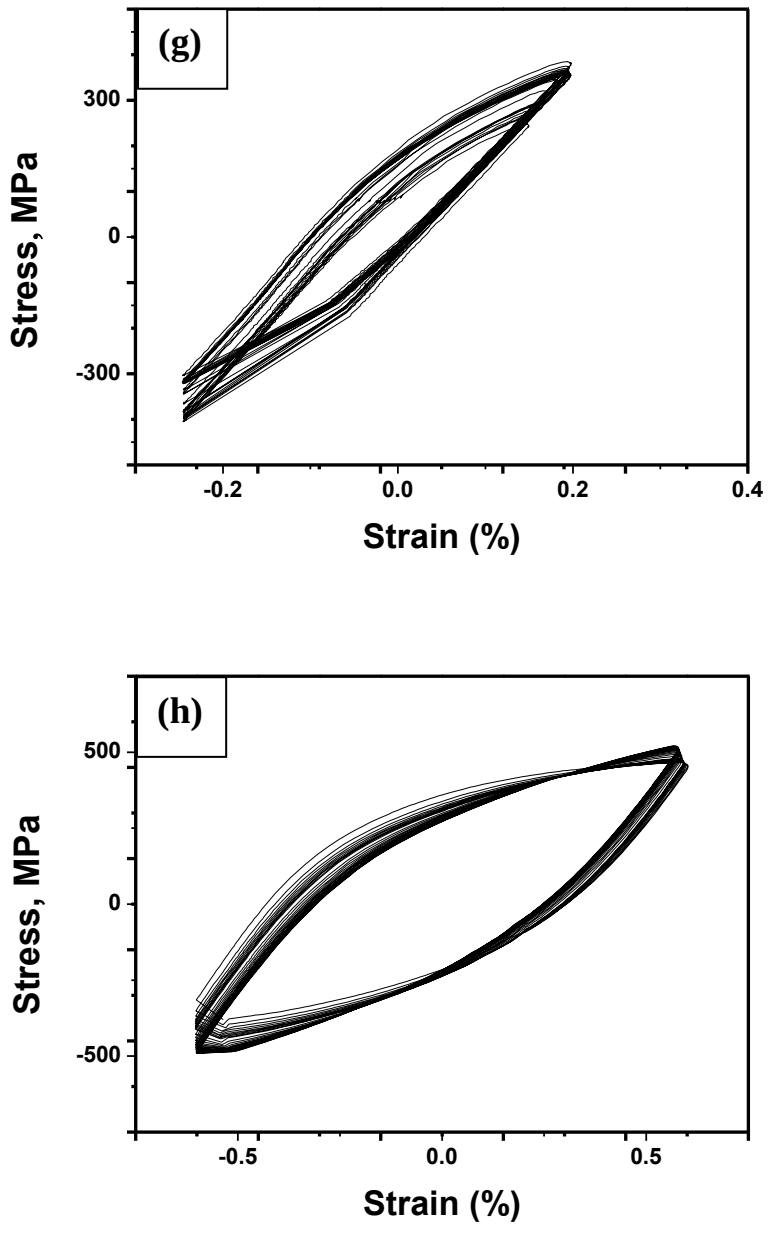

Fig. 4.14: Hysteresis loops generated during a LCF test at (g) stain amplitude (ε_t) of 0.25% and (h) stain amplitude (ε_t) of 0.60% for 7 hours sensitized case.

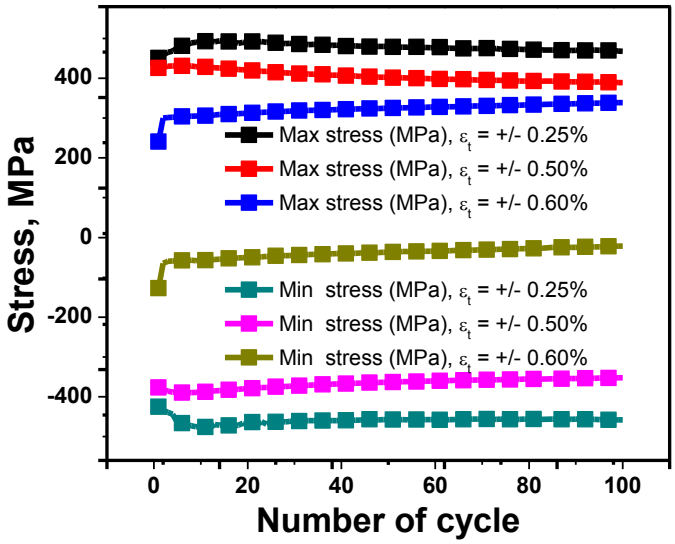

Fig. 4.15: Maximum and minimum stresses vs number of cycle, N for solution annealed steel.

(a)

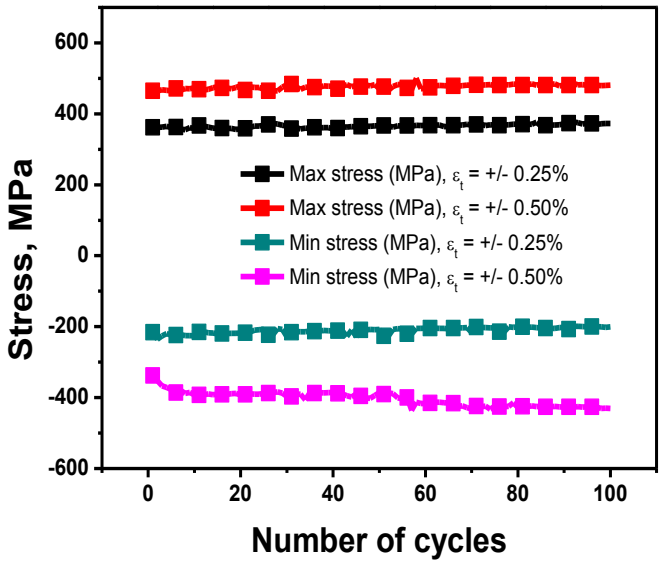

Fig. 4.16: Maximum and minimum stresses vs number of cycle, N for: (a) 1 hrs, (b) 3 hrs, (c) 5 hrs, and (d) 7 hrs sensitized steel.

(b)

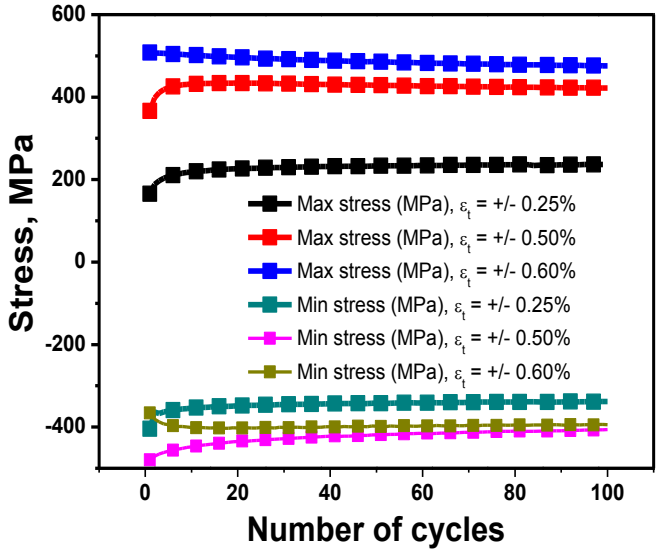

(c)

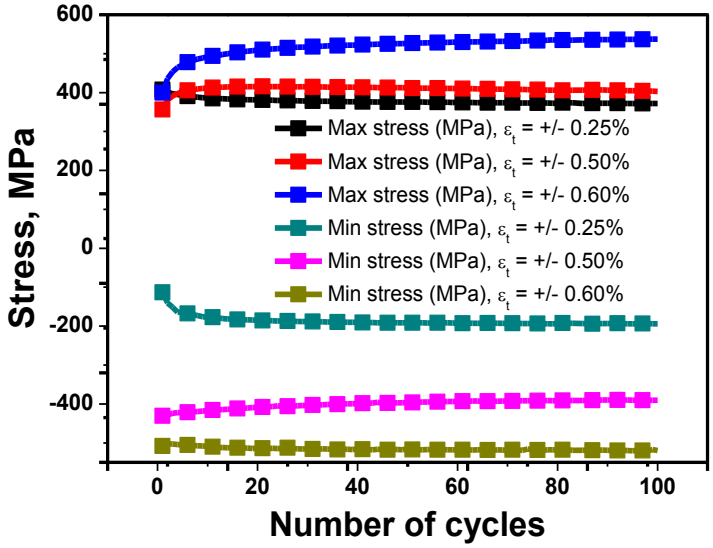

(d)

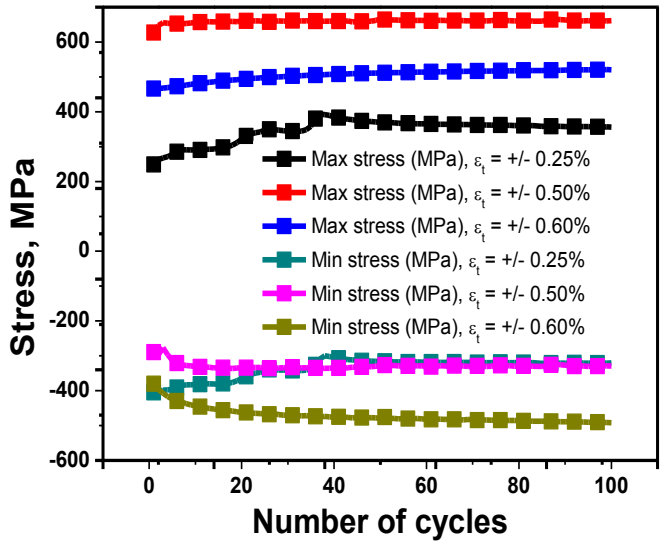

Contd……Fig. 4.16: Maximum and minimum stresses vs number of cycle, N for: (a) 1 hrs, (b) 3 hrs, (c) 5 hrs, and (d) 7 hrs sensitized steel.

4.8 Post-fatigue tensile properties

Tensile tests have been conducted on the same specimens which have been subjected to fatigue damage for 100 cycles to study the tensile properties of investigated non-conventional stainless steel subjected previous cyclic loading. Typical engineering stress- engineering strain plots of the pre-fatigued solution annealed and sensitized stainless steel samples are shown in Fig.4.17- 4.20. One can note that although the variations in yield strength values do not follow any specific trend, the ultimate tensile strength values reduce as that compared with the ultimate tensile strength values of the specimens which have not undergone any previous fatigue cycling.

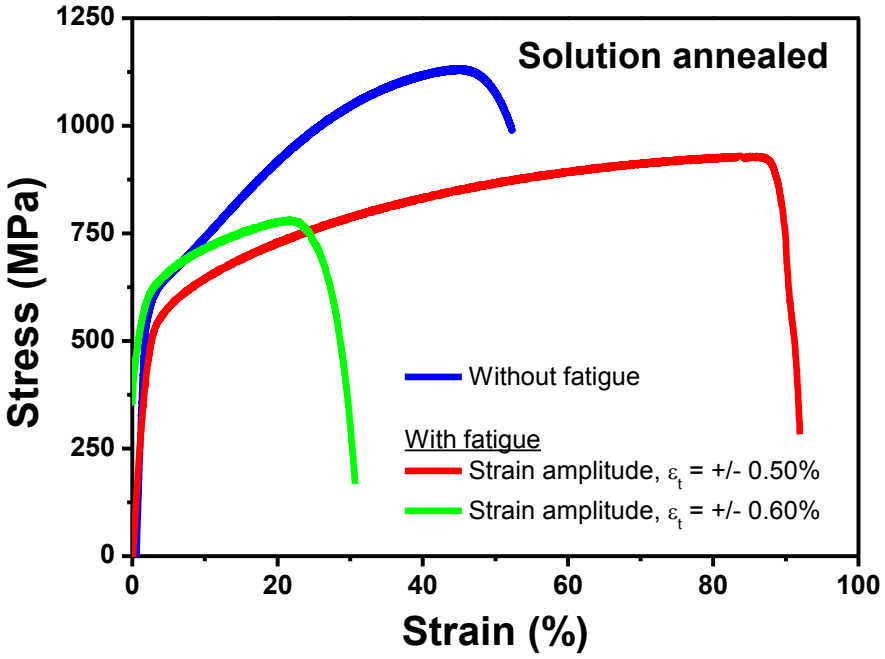

Fig. 4.17: Engineering stress-strain plot of the solution annealed steel with and without fatigue.

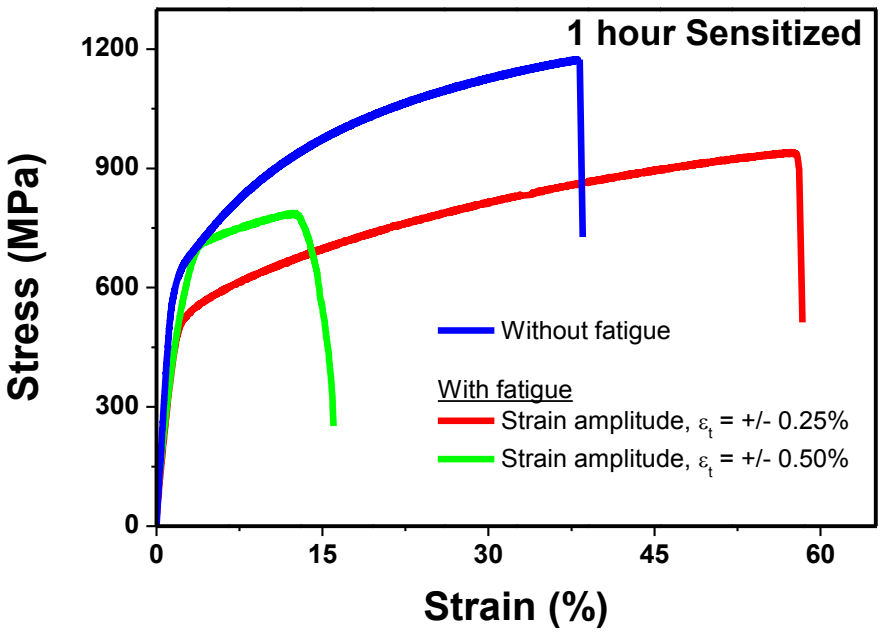

Fig. 4.18: Engineering stress-strain plot of the 1 hour sensitized steel with and without fatigue.

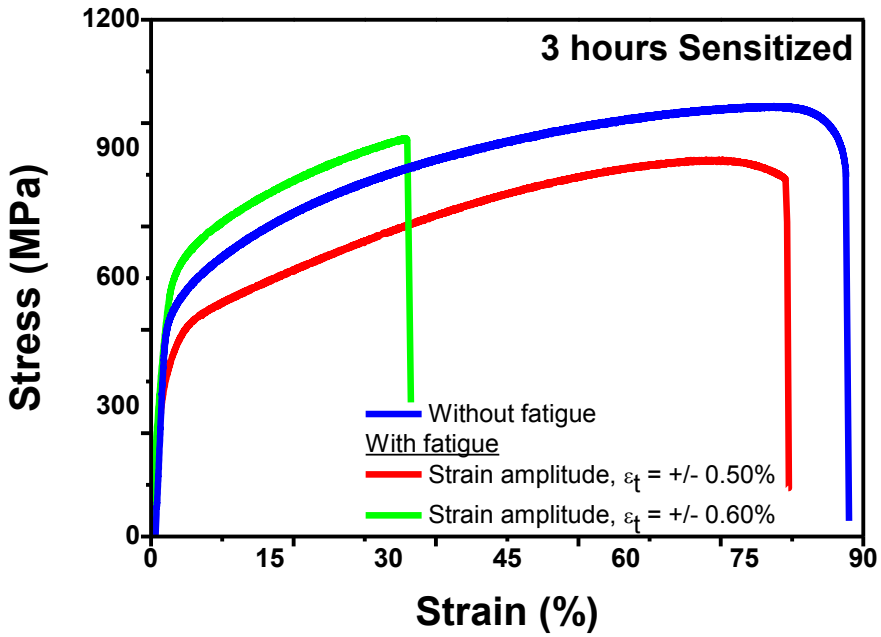

Fig. 4.19: Engineering stress-strain plot of the 3 hours sensitized steel with and without fatigue.

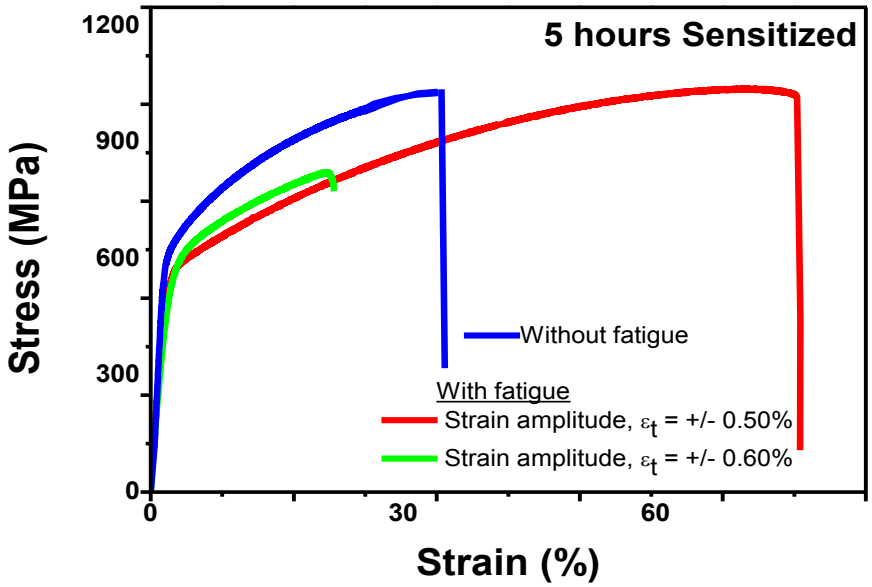

Fig. 4.20: Engineering stress-strain plot of the 5 hours sensitized steel with and without fatigue.

4.9 Fractographic examinations

The fracture surfaces of broken tensile specimens have been observed under the field emission scanning emission microscope. A series of fractographs were taken in order to analyze the nature of fracture morphology. A typical fractograph of solution annealed specimen is shown in Fig. 4. 21 (a), reveals classical dimple morphology as can be anticipated in a ductile material like stainless steel. It is known that mechanism of ductile fracture is composed of three consecutive events such as void nucleation, their growth and finally their coalescences[50-54]. Fracture surface of the solution annealed specimen reveals that it consists different sizes of dimples at different places as shown in Fig. 4.21 (a) by arrow mark. This provides evidence that a few voids were developed substantially during fracture. The fracture surfaces of deformed sensitized specimens were observed in the similar way and found that it is one kind of rock candy fracture (i.e. type of brittle intergranular fracture). It is known that during sensitization effect grain boundaries get embrittled which causes the cracks to propagate through grain boundary thus causing intergranular fracture. It can be seen

that various cracks have been developed in the steel. These cracks are shown by arrow marks embedded on the fracture surface as shown in Fig. 4.21 (b).

As is discussed in the previous paragraph that the basic features of the steel is of ductile nature and therefore a few dimples are present at certain places of the fracture surface. The

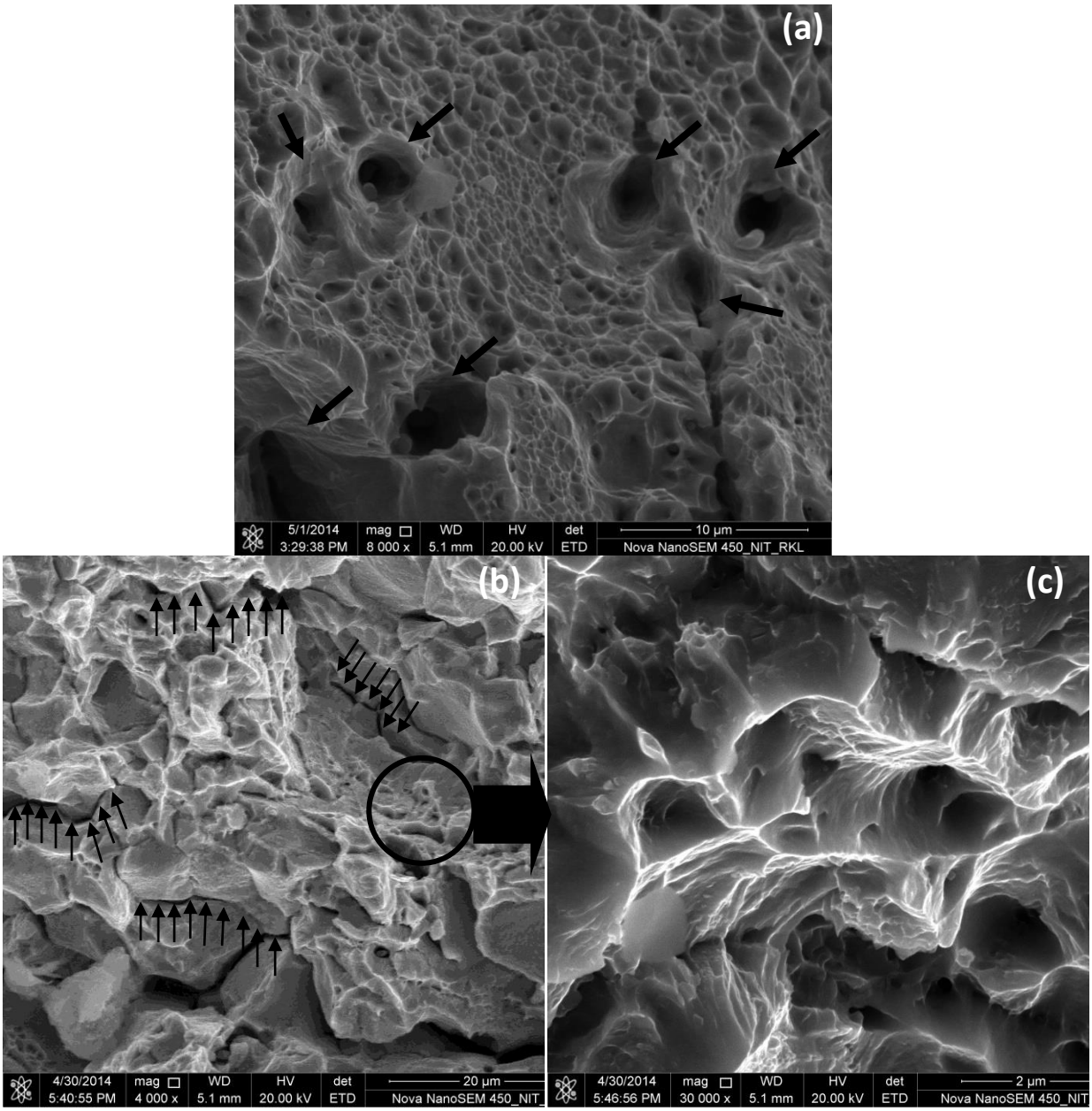

Fig.4.21: (a) A typical tensile fractograph of solution annealed non-conventional stainless steel showing classical dimples, (b) typical fracture surface of the sensitized (1 hr) stainless steel fractured during post-fatigue tensile test (the arrow marks are showing intergranular crack propagation) and (c) dimples present at few places of the 1 hr sensitized specimen taken at higher magnification (circled part of figure b).

region is rounded in Fig. 4.21 (b) and a magnified image of it is illustrated in Fig. 4.21(c). Overall, a detailed comparison of the all sensitized stainless steel fracture surfaces indicates that the fractures are primarily dominated by intergranular fracture with a few features of ductile signatures.

4.10 X-ray diffraction analyses

It is very fact that austenitic stainless steel is metastable upon monotonic and cyclic deformation [55]. So, it can be predicted to occur the same in the selected steel as it deform. It has been seen that literature relevant to this domain is less and less number of idea was found in this area to acquire the nature of microstructural variations upon cyclic loading as time of sensitization increases. A series of X-ray diffraction have been carried out for all the solution annealed, sensitized, and deformed specimens of investigated stainless steel after 100 cycles of loading. The XRD results of solution annealed and sensitized steel do not show any phase transformation during sensitization.

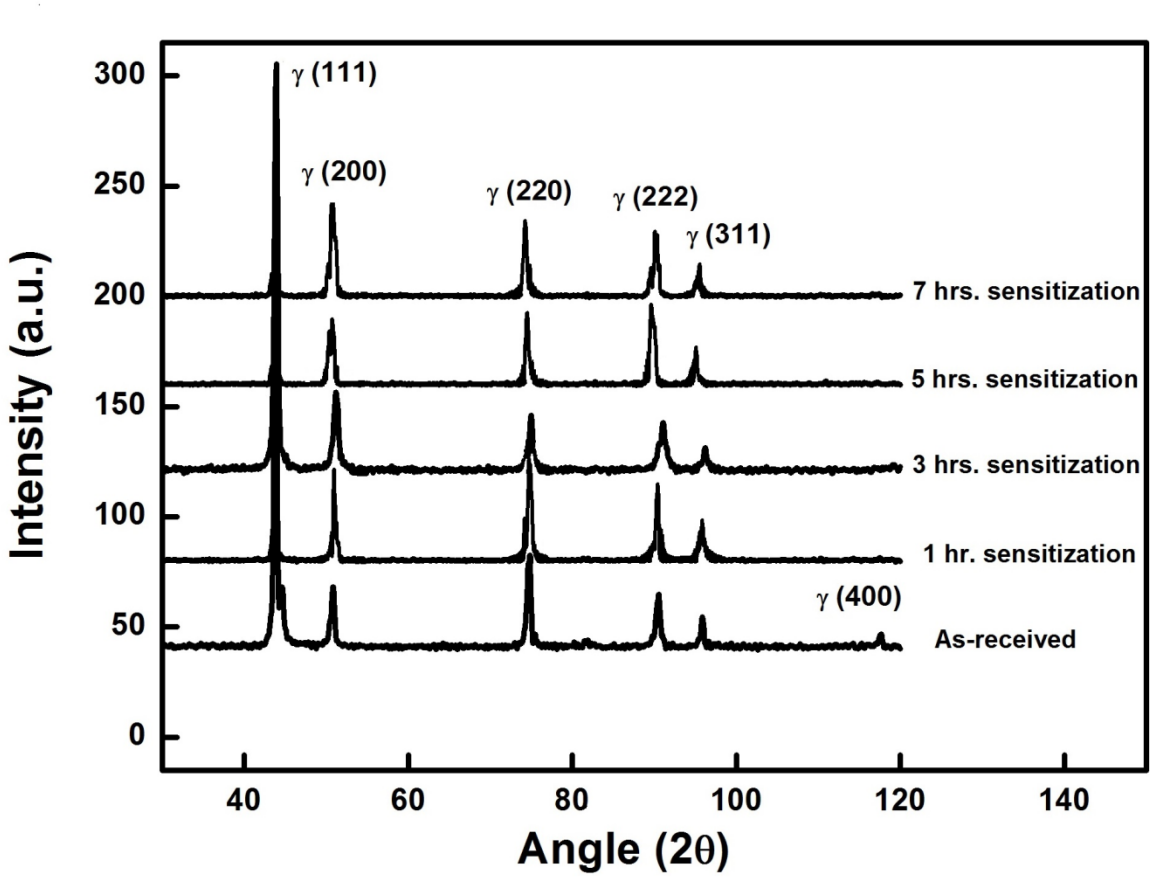

Fig. 4.22:A plot of X-ray diffraction patterns in as-received and the sensitizedconditions subjected to 1, 3, 5, and 7 hours.

However, the XRD profiles show evidences of martensitic transformation in the deformed state. A typical X-ray diffraction plot for the 7 hrs sensitized steel is given in Fig. 4.23, which indicate presence of (200), (211) and (220) peaks of α´ indicating martensitic transformation in the steel in sensitized state.

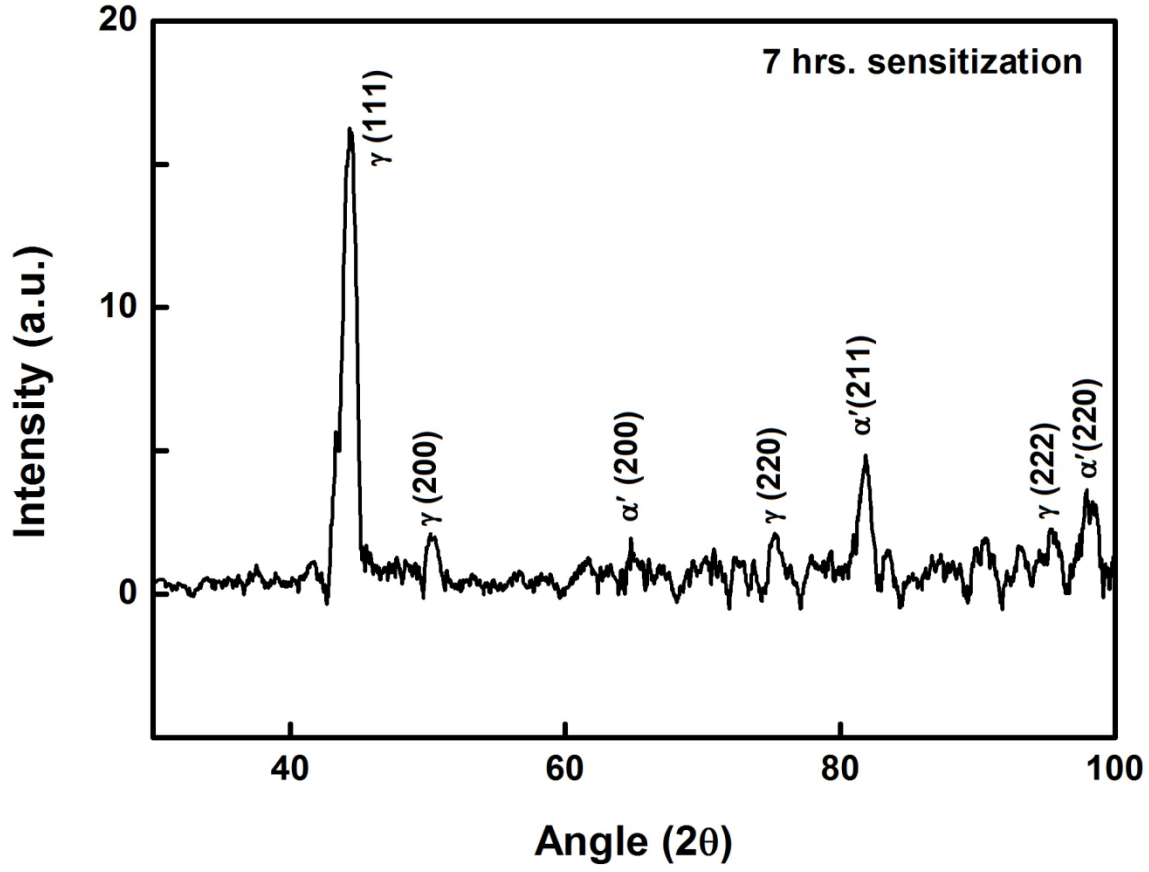

Fig. 4.23:A typical plot of X-ray diffraction pattern of 7 hrs sensitized deformed specimen.

4.11 Estimation of dislocation density

The dislocation densities of the solution annealed, sensitized and deformed specimens have been estimated from X-ray diffraction profile analysis using the method given by Ungár [40].

As per Ungár, the modified Williamson-Hall equation:

$$\Delta K \cong \frac{1}{d} + \left(\frac{\pi M^2 b^2}{2}\right)\rho^{\frac{1}{2}}\left(K^2\overline{C}\right) + O\left(K^4\overline{C}^2\right) \qquad \textbf{(4.1)}$$

Where,

$K = 2\sin\theta/\lambda$

$\Delta K = 2\cos\theta(\Delta 2\theta)/\lambda$

$b =$ Burgers vector of dislocations

$d =$ Average grain size

$\theta =$ Diffraction angle

$\Delta(2\theta) =$ Integral breadth (FWHM) of the peak

$\lambda =$ Wave length of X-rays

$\rho =$ Average dislocation density

M = Effective outer cut-off radius of the dislocation density and dislocations.

The value of M lies between 1 to 2 for deformed materials. So, the value of M was considered 2 for this calculation.

The value of C denotes the average contrast factor of the dislocations. The average contrast factor is calculated by using the relation:

$$C = C_{h00}\left[1 - q\left(\frac{h^2k^2 + k^2l^2 + {}^2h^2}{h^2 + k^2 + l^2}\right)\right] \quad \textbf{(4.2)}$$

Where,

$C_{h00} =$ Average contrast factor equivalent to h00 reflection

The value of C_{h00} =0.266 and q= 2.203 is calculated based on the expressions given in Ungár[43]. Here, due to containing higher order terms in $K^4\overline{C}^2$, therefore the term $O\left(K^4\overline{C}^2\right)$ has been neglected during the calculations.

The XRD profile peaks (111), (200), (220) (222) and (311) have been taken for as-received and sensitized condition while (111), (200), (220), (211), (222) and (220) have been taken for deformed specimens for the calculation. The FWHM (full width half maximum) and θ (diffraction angle) for all peaks were calculated. For all calculations, an average value of Burgers vector (b=0.253 nm) has been taken for the subsequent calculation.

Table 4.6: Dislocation densities obtained from X-ray diffraction profile analyses.

Sample condition / Dislocation density (m^{-2})	Solution annealed	Sensitization			
		1 hr	3 hrs	5 hrs	7 hrs
Before Deformation	6.5076×10^{14}	5.9220×10^{14}	8.6164×10^{14}	9.0575×10^{14}	9.9698×10^{14}
After Deformation	8.1027×10^{15}	6.2245×10^{15}	5.1312×10^{15}	7.0012×10^{15}	6.2804×10^{15}

The obtained value of dislocation densities of solution annealed, sensitized as well as deformed specimens is given in Table 4.6 where it can be seen that deformed specimens have increased by approximately an order of magnitude.

Chapter 5

Conclusions and Scope for future research

Outline

Conclusions

Scope for future research

5.1 Conclusions

The obtained results and their pertinent discussion lead to the following conclusions:

1. The microstructures of the investigated non-conventional stainless steel show equiaxed grains in solution annealed condition. However, the volume of the sensitized grain boundaries increased with sensitization time in the sensitized steel. The yield strength (Y.S), ultimate tensile strength (U.T.S) and macrohardness values reduce with increase in sensitization time.

2. The fractographic features indicate that there is predominantly dimpled fractured in solution annealed condition, which has been taken over by predominantly intergranular fracture in the sensitized state. This fact is attributed to grain boundary embrittlement in the sensitized steel.

3. The low cycle fatigue studies up to 100 cycles indicate the steel experiences cyclic softening behavior over the examined range of strain amplitudes. The post fatigue tensile tests also confirm this phenomenon.

4. The dislocation densities in the deformed specimens are calculated using X-ray diffraction profile analysis which show that the dislocation densities in cyclically loaded specimens increase with increasing strain amplitudes.

5.2 Scope for future research

The present study has generated some information regarding the fatigue and post-fatigue tensile behaviour of a non-conventional stainless steel. A number of directions for future research can be suggested from the experience gained in the present work:

I. Cyclic stress –strain curves can be determined for this material.

II. Some transmission electron microscopic studies can be done to estimate dislocation densities and their distribution.

III. In this investigation the sensitization time was taken only upto 7 hours, however sensitized studies can be done for more hours.

References

[1] Davis, J.R., (Ed.), ASM Speciality Handbook-Stainless Steels, ASM International, USA, (1999).

[2] Levfevre, J., Stainless Steel Selection Criteria for Different Applications, Stainless Steels, Les Editions de Physique, (1993), pp. 919-937.

[3] Gellings, P. J., Dejongh, M. A., Grain boundary oxidation and the chromium depletion theory of intercrystalline corrosion of austenitic stainless steels, Corrosion Science, Vol. 17, (1967), pp. 413-421.

[4] Strauss, B., Schottky, H., Hinnuber J., Carbide formation on annealing stainless, nonmagnetic, Cr-Ni steels, Z. anorg allgem. chem., Vol. 188, (1930), pp. 309.

[5] Stawstrom, C. and Hillert, M., An improved depleted zone theory of intergranular corrosion of 18-8 stainless steel, Journal of Iron and Steel Institute, Vol. 207, (1969), pp. 77 -85.

[6] Tedmon, C. S., Vermilyea D. A., J. H. Rosolowski, Jounal of Electrochemical Society, Vol. 118, (1971), pp. 192.

[7] Fullman, R. L., A thermodynamic model of the effects of composition on the susceptibility of austenitic stainless steels to intergranular stress corrosion cracking, Acta Metallurgica. Vol. 30, (1982), pp. 1407-1415.

[8] Devine, T. M., The mechanism of sensitization of austenitic stainless steel, Corrosion Science, Vol. 30, (1990), pp. 135-151.

[9] Bain, E. C., Aborn, R. H., Rutherford, J. J. B., The nature of preventation of steels, Transaction of the American society for steel treating, Vol. 21, (1933), pp. 481-509.

[10] Leiva-García, R., Akid, R., Greenfield, D., Gittens, J., Muñoz-Portero, M. J., García-Antón, J., Study of the sensitization of a highly alloyed austenitic stainless steel, Alloy 926 (UNS N08926), by means of scanning electrochemical microscopy, Electrochimica Acta, Vol. 70, (2012), pp. 105-111.

[11] Almanza, E., Murr, L. E., A comparison of sensitization kinetics in 304 and 316 stainless steels, Journal of Material Science, Vol. 35, (2000), pp. 3181-3188.

[12] Parvathavarthini, N., Dayal, R. K., Time-temperature-sensitization diagrams and critical cooling rates of different nitrogen containing austenitic steels, Journal of Nuclear Materials, Vol. 399, (2010), pp. 62-67.

[13] Dayal, R. K., Parvathavarthini, N., Raj, B., Influence of metallurgical variables on sensitization kinetics in austenitic stainless steels, International Materials Reviews, Vol. 503, (2005), pp. 129-155.

[14] Dayal, R. K., Gnanamoorthy, J. B., Srinivasan, G., Esaklul K. A. (Ed.), ASM Handbook of Case Histories in Failure Analysis, ASM International, Vol. 2, (1993), pp. 506–508.

[15] Kasivisvanathan, K. V., Muraleedharan, N. G., Raghu, N., Dayal R. K., Shaikh, H., Khatak, H. S., Baldev Raj (Eds.), Corrosion of Austenitic Stainless Steels – Mechanism Mitigation and Monitoring, Narosa publishing house, New Delhi, (2002), pp. 314–339.

[16] Das, C. R., Bhaduri, A. K., Ray, S. K., Fatigue failure of a fillet welded nozzle joint, Engineering failure analysis, Vol. 10, (2003) pp. 667–674.

[17] Dayal, R. K., Gnanamoorthy, J.B., Chandrasekharan, N., Esaklul K. A., (Ed.), ASM Handbook of Case Histories in Failure Analysis, ASM International, Vol. 2, (1993), pp. 253–255.

[18] Hall, E. L., Briant, C.L., Chromium depletion in the vicinity of carbides in sensitized austenitic stainless steels, Metallurgical transaction A, Vol. 154, (1984), pp. 793-811.

[19] Dutta, R. S., De, P. K., Gadiyar, H. S., The sensitization and stress corrosion cracking of nitrogen-containing stainless steels, Corrosion Science, Vol. 34, (1993), pp. 51–60.

[20] ASM International Handbook Committee, Fatigue and fracture, ASM International, USA, Vol. 19, (1996).

[21] Ellyin, F., Fatigue Damage, crack growth and life Prediction, first edition, Chapman & Hall, UK (1997).

[22] Dieter, G. E., Mechanical Metallurgy, SI metric edition, McGraw-Hill Book Company, Singapore (1987).

[23] Hertzberg, R.W., Deformation and Fracture Mechanics of Engineering Materials, third edition, John Wiley & Sons, Singapore (1989).

[24] Suresh, S., Fatigue of Materials, second edition, Cambridge University Press, UK (1998).

[25] Qian, G., Hong, Y., Zhou, C., Investigation of high cycle and Very –High-Cycle Fatigue behaviors for a structural steel with smooth and notched specimens, Engineering failure analysis, Vol. 17, (2010), pp. 1517-1525.

[26] Stanzl-Tschegg, S., Very high cycle fatigue measuring techniques, International Journal of Fatigue, Vol. 60, (2014), pp. 2-17.

[27] Pyttel, B., Schwerdt, D., Berger, C., Very high cycle fatigue- Is there a fatigue limit? , International Journal of Fatigue, Vol. 33, (2011), pp. 49-58.

[28] Shiozawa, K., Hasegawa, T., Kashiwagi, Y., Lu, L., Very high cycle fatigue properties of bearing steel under axial loading condation, International Journal of Fatigue, Vol. 31, (2009), pp. 880-888.

[29] Satyadevi, A., Sivakumar, S. M.,Bhattacharya, S. S., A new failure criterion for materials exhibiting racheting during very low cycle fatigue, Materials Science and Engineering A, Vol. 452-453, (2007), pp. 380-385.

[30] Ghosh, S., Kain, V., Ray, A., Roy, H., Sivaprasad, S., Tarafder, S., Ray, K. K., Deterioration in fracture toughness of 304N austenitic stainless steel due to sensitization, Metallurgical and materials transactions A, Vol. 40A, (2009), pp. 2938-49.

[31] Jones, R., Randle V., Sensitization behavior of grain boundary engineered austenitic stainless steel, Materials Science and Engineering A, Vol. 527, (2010), pp. 4275-4280.

[32] Bruemmer, S. M., Was, G. S., Microstructural and microchemical mechanisms controlling intergranular stress corrosion cracking in light-water-reactor systems, Journal of nuclear materials, Vol. 216, (1994), pp. 348-263.

[33] Yin, Y.F., Faulkner R.G., Model predictions of grain boundary chromium depletion in Inconel 690, Corrosion Science, Vol. 49, (2007), pp. 2177–2197.

[34] Was G.S., Rajan, V.B., The mechanism of intergranular cracking of Ni-Cr-Fe alloys in sodium tetrathionate, Metallurgical Transactions A., Vol. 18, (1987), pp. 1313‑1323.

[35] Watanabe, T., An approach to gain grain boundary design for strong and ductile polycrystals, Research Mechanica, Vol. 11, (1984), pp. 47–84.

[36] Randle, V., Twinning-related grain boundary engineering, Acta Materialia, Vol. 52, (2004), pp. 4067–4081.

[37] Randle, V., Mechanism of twinning-induced grain boundary engineering in low stacking-fault energy materials, Acta Materialia, Vol. 47, (1999), pp. 4187–4196.

[38] Ray, K. K., Dutta, K., Sivaprasad, S., Tarafder, S., Fatigue damage of AISI 304LN stainless steel: Role of mean stress, Procedia Engineering, Vol.2, (2010), pp. 1805-1813.

[39] Ye, D., Matsuoka, S., Nagashima, N., Suzuki, N., The low cycle fatigue deformation and final fracture behaviour of an austenitic stainless steel, Material Science and Engineering A, Vol. 415, (2006), pp. 104-117.

[40] Ungár, T., Dislocation densities, arrangements and character from X-ray diffraction experiments, Material Science and Engineering A, Vol. 309–310, (2001), pp. 14–22.

[41] Renzetti, R. A., Sandim, H. R. Z., Bolmaro, R. E., Suzuki, P. A., Möslang, P. A., X-ray evaluation of dislocation density in ODS-Eurofer steel, Material Science and Engineering A, Vol. 534, (2012), pp. 142–146.

[42] Hecker, S. S., Stout, M. G., Staudhammer. K. P. and Smith, J. L., Effects of strain state and strain rate on deformation-induced transformation in 304 stainless steel. Part I – magnetic measurements and mechanical behaviour, Metallurgical and materials transactions A, Vol. 13A, (1982), pp. 619–626.

[43] E 112-04, Standard Test Methods for Determining Average Grain Size, Annual Book of ASTM Standards, Vol. 03.01, (2004), ASTM, Philadelphia, PA.

[44] E8M-09, Standard Test Methods for Tension Testing of Metallic Materials, Annual Book of ASTM Standards, Vol. 03.01, (2009), ASTM, Philadelphia, PA.

[45] Kishor, R., Sahu, L., Dutta, K., Mondal, A. K., Assessment of dislocation density in asymmetrically cyclic loaded non-conventional stainless steel using X-ray diffraction profile analysis, Materials Science and Engineering A, Vol. 598, (2014), pp. 299-303.

[46] Nayar, A., The steel hand book, second edition, Tata MC Graw- Hill company limited, (2000).

[47] E 112-04, Standard Test Methods for Determining Average Grain Size, Annual Book of ASTM Standards, Vol. 03.01, ASTM, Philadelphia, PA, (2004).

[48] E 8M-08, Standard Test Methods for Tension Testing of Metallic Materials, Annual Book of ASTM Standards, Vol. 03.01, ASTM, Philadelphia, PA, (2008).

[49] Lopamudra sahu, Mech Thesis, Submitted at National Institute of Technology, Rourkela, (2013).

[50] Tvergaard, V., Ductile fracture by cavity nucleation between larger voids, Journal of Mechanics and Physics of Solids, Vol. 30, No. 4, (1982), pp. 265–286.

[51] Thomason, P. F, Ductile fracture by the growth and coalescence of microvoids of non-uniform size and spacing, Acta Materialia, mater. Vol. 41, No. 7, (1993), pp. 2127-2134.

[52] Bandstra, J. P., Koss. D. A, Modeling the ductile fracture process of void coalescence by void-sheet formation, Materials Science and Engineering A, Vol.319–321, (2001), pp. 490–495.

[53] Benzerga, A. A., Besson, J., Pineau, Anisotropic ductile fracture Part II: theory, Acta Materialia, Vol. 52, (2004), pp. 4639–4650.

[54] Bandstraa, J. P., Kossb, D. A., Maticc, A. P., Everettd, R. K., Modeling void coalescence during ductile fracture of a steel, Materials Science and Engineering A, Vol.366, (2004), pp. 269–281.

[55] De, A. K., Murdock, D. C., Mataya, M. C., Speer, J. G. and Matlock, D. K., Quantitative measurement of deformation-induced martensite in 304 stainless steel by X-ray diffraction, Scripta Materialia, Vol. 50, (2000), pp. 1445–1449.